LARGE FORCE SHAPE MEMORY ALLOY LINEAR ACTUATOR

By

JOSÉ R. SANTIAGO ANADÓN

A THESIS PRESENTED TO THE GRADUATE SCHOOL
OF THE UNIVERSITY OF FLORIDA IN PARTIAL FULFILLMENT
OF THE REQUIREMENTS FOR THE DEGREE OF
MASTER OF SCIENCE

UNIVERSITY OF FLORIDA

2002

To my parents, to whom I owe my dreams and spirit.

ACKNOWLEDGMENTS

I would like to thank my chairman, Dr. Carl D. Crane III, for his support and encouragement throughout the years in this research. Additional thanks go to the members of the committee, Dr. Ashok Kumar, Dr. Nagaraj Arakere, and a special mention goes to Dr. Paul Mason, who also supported me, and to the Department of Mechanical Engineering of the University of Florida for giving me the chance of working there in the first place. The help of several of the graduate students at the Center for Intelligent Machines and Robotics (CIMAR) was greatly appreciated. Among them a special mention goes to Shannon Ridgeway, Anthony Hinson, Arfath Pasha and Chris Fulmer, all of whom contributed to this work.

TABLE OF CONTENTS

page

LIST OF TABLES

Table page

LIST OF FIGURES

Figure page

Abstract of Thesis Presented to the Graduate School
of the University of Florida in Partial Fulfillment of the
Requirements for the Degree of Master of Science

LARGE FORCE SHAPE MEMORY ALLOY LINEAR ACTUATOR

By

José R. Santiago Anadón

August 2002

Chair: Dr. Carl D. Crane III
Department: Mechanical Engineering

The design and development of a linear actuator for macro devices using shape memory alloy (SMA) are desired. The implementation of shape memory alloys for large scale applications has mainly three major drawbacks: strain constraints, limited cycles and the actual usable force. This work will address two out of these three: the amount of force and cycles. A parallel array of shape memory alloy wires working in unison was implemented. The final prototype was capable of lifting more than 100 lbs with a stroke of 0.80 inches. A PID controller was designed, implemented and tested for the actuator and response data for different loading conditions, and setpoints were collected.

CHAPTER 1
INTRODUCTION

As technology advances, the building blocks that drive it remain relatively unchanged. Motors, as were 100 years ago, are still being employed today as the preferred devices for actuation and applications where the use of motors proves to be unpractical are in some cases left behind or unexplored. In some instances a new revolutionary technology comes along opening the door for new ideas and designs and with it, what seems unfeasible in the past becomes now challenging. Think of all the engineering and science problems that were thought of before the advent of computers and discarded because of the intensive calculations that they required. Today we look at calculation intensive problems on a daily basis and the main tool for solving them is the computer.

Although not as revolutionary as computers, shape memory alloys have proven their worth in solving engineering problems that in the past seem implausible. Only a few decades old, this new breed of driving mechanism has a bright future ahead. The main reason behind their importance today is simple; shape memory elements provide a significant amount of actuation with an extremely small envelope volume. This statement becomes truer and their implementation even more important when looking at the direction where technology is heading. In the modern world great emphasis has been placed in miniaturization. Micro devices are being developed and implemented today to perform a multitude of tasks with nano technology following very closely behind. These machines can then be used for a multitude of applications such as robotics, biomechanics,

surgery, transportation vehicles, computer components, and recognizance and survey devices.

Another advantage that shape memory alloys have over conventional actuation mechanisms is their versatility. A shape memory element can be actuated thermally or electrically. Not having to rely on moving parts for actuation, just the simple contraction of the material, makes them highly attractive for actuation where low or no noise levels are desired. Besides being an actuator they can also serve as thermal sensors and superelastic springs. Some existing applications use them as an actuator and a sensory device, thus minimizing space and cost for the designer. The most popular incarnation of shape memory alloys, Ni-Ti, is biocompatible.

So far though, mainly because of efficiency concerns, shape memory alloys have yet to be adopted fully in large-scale applications. Albeit that they do have a tough competition with hydraulics, electrical motors, and internal combustion engines to go against them, there are large-scale applications that would benefit from their use, especially when size is a major design factor to consider. Although part of a chapter of this work has been dedicated to these applications, a few of these applications are named now to keep the scope of this research in context. The most logical application area for a large-scale shape memory alloy actuator is biomechanics. A person that has lost an arm for example can have a lightweight but incredibly powerful prosthesis without the need of motors or compressors. Macro scale shape memory actuators can also be implemented in situations where accessibility to the operation site is limited but when large amounts of work are required. Aerospace is another field that benefits from these devices

minimizing the space and weight of a would-be actuator. In fact shape memory alloys have already reached Mars as part of one of the mechanisms of NASA Mars Pathfinder.

This work focuses on the design and development of a large-scale shape memory linear actuator. A design procedure was created which takes into account all the correlations that exist in the design parameters and actuator properties. This procedure serves as the basis for the development of the final prototype. Several prototypes were designed; each one with a different approach as to the implementation of the shape memory elements and one of these prototypes was built and tested.

Shape Memory Basics

The basics of memory materials have been extensively documented by numerous papers and it is not the intention of this research to expand on this area, but rather than to give the reader a primer into the subject to better understand latter topics.

The term shape memory alloy indicates a material that has the ability to deform to a preset shape when heated and in the process perform a useful engineering function. There are five documented functions that a SMA can deliver [1]:

1. *Free recovery* describes a SMA element whose sole function is to cause a displacement. Since no work is being produced this kind of application is mostly used in control devices and relay mechanisms.

2. In *constrained recovery* the element is prevented from displacement generating large amount of stresses. This type of function is being used increasingly in fittings, couplings and connectors for machinery.

3. When used as an *Actuator*, the SMA element produces work that is force coupled with displacement. A vast majority of applications employ SMA in this fashion. Tini Aerospace has had great success developing shape memory actuators for space applications. Currently the company offers three major actuators (Figure 1.1): The Frangibolt actuator uses a SMA cylinder to elongate and in the process fracture a bolting element with forces up to 5000 lbf, which upon release deploys a structure. The other two actuators provide linear and rotational motion.

4. *Superelasticity* behavior makes the SMA function as an enhanced spring with a high elastic deformation. The most common example for this shape memory effect is employed in eyeglass frames (Figure 1.2) that can be subject to a large deformation and when released they will return to the original shape.

5. *High damping* capacity in the martensite state. Memry Corp. developed a new type of shape memory alloy named Zeemet® with high damping properties for use as inserts in golf wedges and putters (Figure 1.3). The benefits to the golfer when using a SMA club includes an increased spin on the ball, greater control and solid feel.

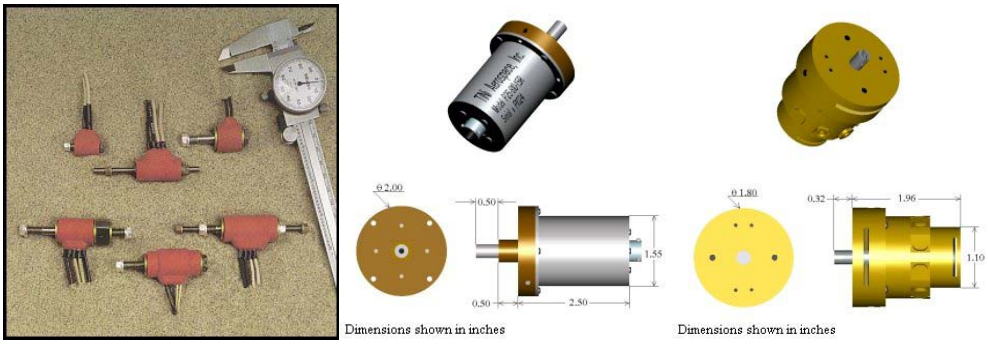

Figure 1.1 TiniAerospace shape memory actuators. From left to right: Frangibolt, Pinpuller, and Rotary Actuator.

Figure 1.2 Superelastic eye frames.

Figure 1.3 Shape memory alloy golf clubs.

Martensitic Transformations

In general, the shape memory event is based on the ability of the material to change its crystal structure, in other words transforming from one crystal structure to another. In shape memory alloys this transformation is usually referred to as a martensitic transformation. The term martensite takes its name from Adolf Martens (1850-1914) a German metallurgist who first discovered this structure in steels. Later it was discovered that this transformation between austenite and martensite phases was not limited to steel [2].

When a material changes phase the rearranging of atoms that takes place is referred to as a transformation. In solids there are two known types of transformations: displacive and diffusional. In a diffusional transformation the rearranging of atoms occurs across long distances. The new phase formed by a diffusional transformation is of different chemical composition than that of the parent phase. In contrast, a displacive transformation occurs by the movement of atoms as a unit, with each atom contributing a small portion of the overall displacement. In a displacive transformation the bonds between the atoms are not broken rather than arranged, thus leaving the parent phase chemical composition matrix intact. Martensitic transformations in shape memory alloys are of displacive type and transformation takes place between Austenite also usually referred to as the parent phase and Martensite. Duerig et al. [3] categorizes the austenite to martensite transformation into two parts: Bain Strain and lattice-invariant shear. The Bain Strain takes its name from Bain who in 1924 proposed it and refers to the necessary deformation needed to obtain the new atomic structure. A two dimensional representation of the Bain Strain is shown in Figure 1.4.

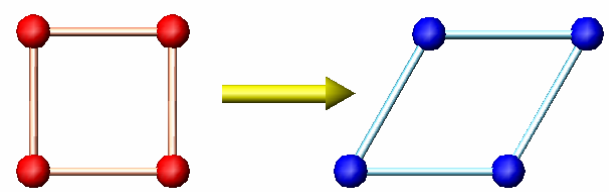

Figure 1-4 Lattice deformation required for changing crystal structure.

The second step of the martensitic transformation depicts the accommodation process required as a result of shape change. This process of accommodation called lattice invariant shear can be accomplished in two ways: slip and twinning (Figure 1.5).

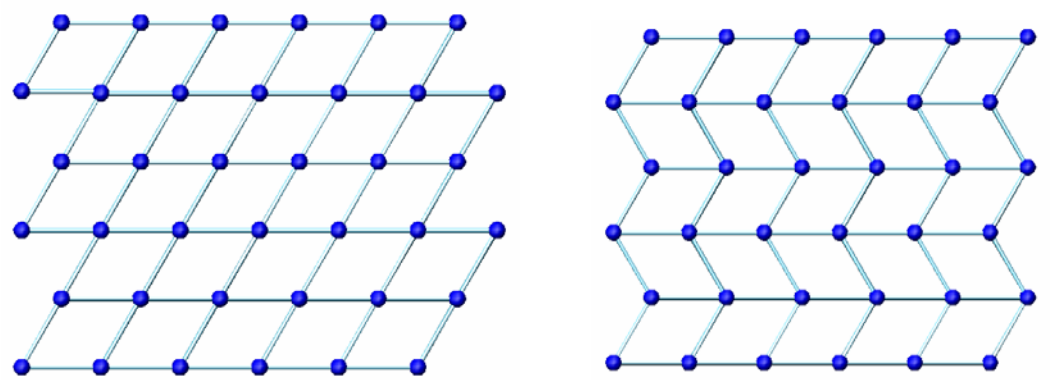

Figure 1.5 Lattice invariant shear accommodation by slip (left) and twinning (right).

Slipping does not preserve all the bonds between the unit atomic cells in the martensite making the transformation irreversible. On the other hand, twinning is a reversible process that allows the material to transform back to its parent phase. Since shape memory behavior is a reversible process the accommodation mechanism that takes place in them is twinning. The mirroring plane on which twinning occurs is usually termed the twin boundary. Figure 1.6 depicts a twinned martensite state on which the order of the atoms is inherited from the austenite. Since twin boundaries can be readily moved, the inclusion of an external shear stress can alter the twinned martensitic state of the matrix to reflect only one variant of twinning as shown on Figure 1.7.

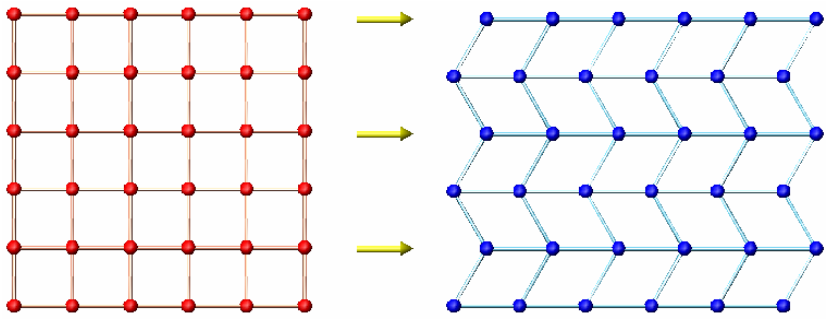

Figure 1.6 Inherited order of atoms during martensite formation.

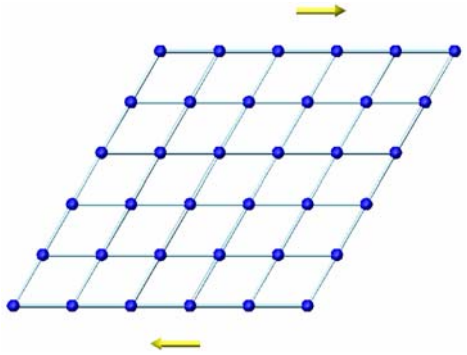

Figure 1.7 De-twinned or deformed martensite by the inclusion of shear stress.

Although the previous review introduces the reader to the shape memory internals, it does not tell the entire picture. In practical terms the behavior mentioned above is related to the temperature of the shape memory element, which determines its crystallographic state. A typical shape memory element has four relevant temperatures that define the different stages of actuation, thus providing the designer a method for control. Simply put, the four temperatures define the start and finish transformations for martensite and austenite (Figure 1.8). In ascending order these temperatures and abbreviations are as follows:

1. Martensite Finish (Mf)
2. Martensite Start (Ms)
3. Austenite Start (As)
4. Austenite Finish (Af)

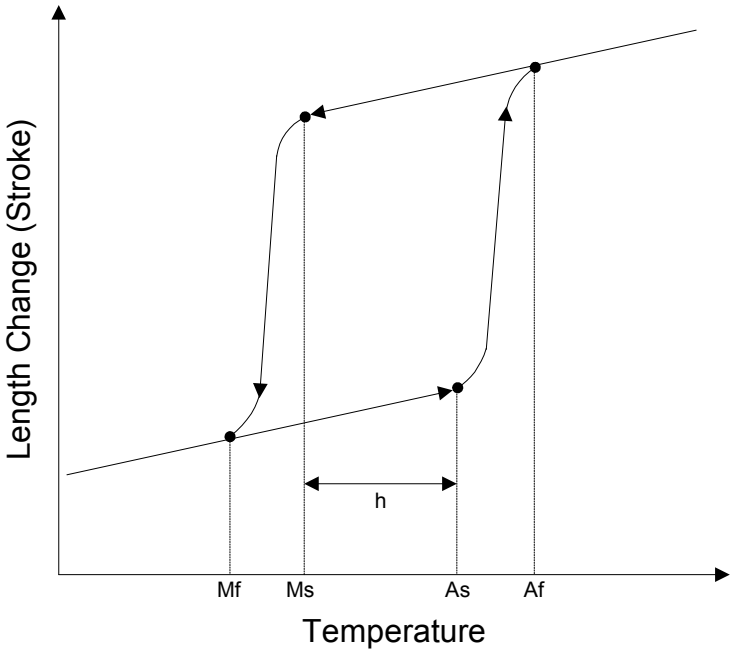

Figure 1.8 SMA Length vs. Temperature Schematic.

Another important factor to notice is that shape memory alloy incurs a temperature hysteresis between its martensite and austenite states. Due to this hysteresis the transformation from martensite to austenite will not coincide with that from austenite to martensite and hence the importance of the four temperatures. The presence of the hysteresis also provides a control challenge for the designer.

The Shape Memory Effect

In order for an alloy to exhibit shape memory behavior certain conditions must be met. Specific weight percentages of each element must be combined in a precise fashion to produce a shape memory viable material. Additional processes enhance material properties and define their shape setting characteristics. Depending on the processing technique used a shape memory element can display one of five distinct shape memory behaviors. These effects are discussed next.

One-Way Memory

This is the most basic form of shape memory and hence the most adopted due to the lower amount of processing that goes into the material, which translates to a reduced cost. This type of effect can be described by its operation cycle outlined below.

A shape memory as-drawn wire initially in its martensite phase has a temperature equal or lower than the martensite finish temperature (Mf). Microscopically the element will have the material martensitic unit atomic structure[1] and an untwinned or deformed matrix structure; macroscopically the element will be in its relaxed state. If the temperature of the element is gradually raised at some point austenite will begin to form in the element, hence the name austenite start temperature (As). Austenitic structures will begin appearing in the once fully martensite and as the temperature raises the percentage of austenite will increase as well. Physically the wire will start to compress and if designed for, produce work. The austenite finish temperature marks the end of the austenitic transformation. At this point the matrix is fully of austenitic atomic structure and a wire with a reduced length should be noticed. The material temperature is now lowered until it reaches the temperature known as martensite finish (Mf). In the same way as austenite before, the material will start reverting to its martensite state. The orientation of the martensite crystals will be in a twinned fashion with an inherited order from the austenite and multiple variations as to accommodate whatever volume the austenite once occupied. Eventually the element will cool furthermore until it reaches the Martensite Finish temperature (Mf) again. Despite the fact that the material completed a

[1] Shape memory alloys atomic structures can vary greatly. For purposes of simplification the schematics presented in this work are assumed as cubic for austenite state and rhombohedral for martensite.

full cycle, at least temperature-wise, a full actuation cycle requires a reset force to deform the martensite back to a uniform favored variant of atomic structure and an untwinned martensite state. If no reset force is applied during the cooling process, the shape of the material will not change and is only the inclusion of this force that an observable elongation in the wire should be noted. Once the untwinned martensite has been forced the cycle can begin again.

The bias force will also gradually decrease as the actuator performs more cycles. The general concept behind this behavior, termed walking, relies on the ability of the material to also remember its martensitic deformed state. Walking is a form of the next memory effect to be discussed called two-way memory with the only difference being that the material learns the behavior during processing instead of operation.

Two-Way Memory

On a two-way memory actuator the inclusion of the external stress can be lowered and in some cases not needed at all due to the fact that the alloy will, upon reaching Mf, revert to its original deformed martensite shape. In two-way systems the amount of work that the alloy is capable of producing during the falling cycle (martensite transformation) is minimal and no loading is recommended at this stage. In fact this type of memory setting is only used to reduce or dismiss the biasing force completely. Perkins and Hodgson [4] describe this effect in more detail and give processing methods on how to obtain alloys that will exhibit the two-way effect. Ryhänen [5] describes two methods for obtaining two-way memory.

All Around Memory Effect

Depending on the composition and processing of the alloy a special case of two-way memory has been found and termed all-around memory effect. The most telling

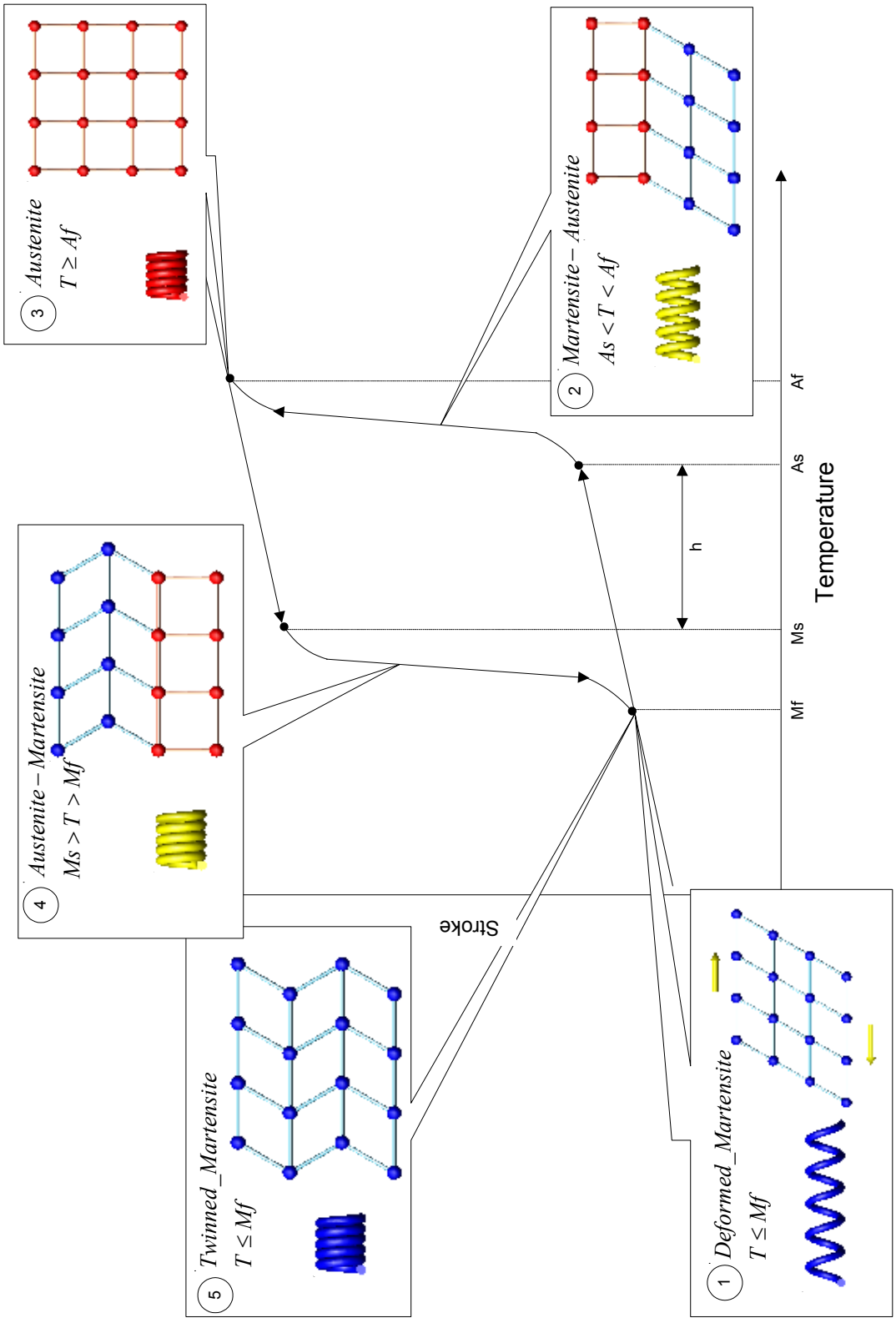

Figure 1.9 One way shape memory effect.

feature of this type of memory is that the low and high temperature shapes are complete opposites. Perkins and Hodgson also describe this effect in more detail [4]. The following was taken from Shape Memory Alloys [2] on which Funabuko gives a general technique for obtaining this type of memory effect for binary Ni-Ti:

1. Deform the martensite beyond the limit.
2. Deform the parent phase more than is possible in a stress induced martensite transformation.
3. Deform the parent phase, cool the specimen to below the Mf temperature under restriction, and maintain this under stress for a long period of time.
4. Deform the martensite phase, heat the specimen under restriction, and induce the reverse transformation.
5. Deform the specimen after creating minute precipitates in the parent phase.

R-Phase Transformation

Besides the martensite - austenite transformation there exists one more noticeable transformation in shape memory alloys. When an alloy is cooled down from Af the material can transform from an austenite cubic to a rhombohedral lattice structure, which is why the name R-Phase transformation. The most noticeable drawback of using this type of transition is that the strain associated with this transformation is rather small, only 0.5%. The temperature hysteresis can be as low as 1.5°C and that makes them ideal for high cycle rate thermally controlled actuators. It has been proved that these kinds of actuators suffer less from fatigue and can yield millions of cycles before failing or degrading. Several researchers have described this effect in more detail including Otsuka [6] and Suzuki and Tamura [7], who describe the fatigue properties.

Superelasticity

Every one of the shape memory effects described above requires a temperature change to precipitate the transformation. There exists, however, a special memory effect under which no temperature change is needed called superelasticity. When superelasticity is present in a SMA the martensite state is induced by an external applied stress. When the stress is released the material reverts back to its austenite state. For the material to exhibit superelasticity it must be designed to have an Austenite finish temperature near the operating temperature, this in most cases would be ambient. Duerig and Zadno [8] explain this effect in more detail.

Shape Memory Materials

There a numerous alloys that exhibit shape memory but overall there are two which are commercially available due in part for their proven ability to excel in some design aspects like maximum strain achievable, biocompatibility, lifespan etc. Table 1.1 [3] shows the different kinds of alloys and their commercial availability.

Table 1.1 Shape Memory Materials.

Alloy	Commercially Available
Au-Zd	No
Cu-Zn	No
Ln-Ti	No
Ni-Ti	Yes
Cu-Zn-Al	Yes
Ti-Nb	No
Au-Cu-Zn	No
Cu-Zn-Sn	No
Cu-Zn-Si	No
Cu-Al-Ni	Yes
Ag-Cd	No
Cu-Sn	No
Cu-Zn-Ga	No
Ni-Al	No
Fe-Pt	No
U-Nb	No
Tl-Pd-Ni	No
Fe-Mn-Si	No

Ni-Ti (Nitinol)

Nitinol takes its name from Nickel-Titanium for its composition and NOL from Naval Ordinance Laboratory, which is the place where they first discovered its shape memory aspects. Today Ni-Ti is the most common commercially available shape memory alloy and for good reason. The maximum strain that can be obtained from this kind of alloy reaches 8%. This is a high number under SMA standards since most of the alloys only achieve between 2 to 4% strain. Its biocompatibility makes them attractive for medical applications. The only drawback lies on its cost, which is substantially higher than its peers.

Ni-Ti-Cu

Although Ni-Ti is the most common standard shape memory alloy available some of its properties might not be adept for specific designs. Because of this, extensive research has been conducted to improve some of its mechanical properties. One of the methods of doing this is by adding a ternary element to Ni-Ti. Cu addition to Ni-Ti lowers the martensite phase yield strength of the material and produces a smaller temperature hysteresis when compared to Ni-Ti. Lower yield strength on the martensite phase will decrease the amount of bias force required to deform the SMA element in that phase thus providing a higher net output force. The smaller temperature hysteresis provides faster actuation times or cycle rates, it can also make the actuator more suitable for thermal actuation.

CHAPTER 2
LITERATURE REVIEW

The nature of shape memory design requires that the designer have a vast understanding of the subject. The role of this review is twofold: to provide the user with common accepted background and computational procedures that relate to shape memory design and a review of current devices similar to the one proposed.

Shape Setting Calculations

One of the main advantages of using shape memory alloys is the fact that they can be set to take any form the designer imparts on them. In reality because of the cost of shape setting and the limitations in force and stroke, non-conventional shapes are not used very often. Instead more conventional, mass produced shapes are usually employed. The most common of the conventional shapes are wire, ribbon or strip, and springs. This section will discuss these shapes in more detail and review accepted design methodologies.

As Drawn Wire

Wire is the most common form of shape memory alloy. When compared to other forms it provides the maximum amount of force per cross sectional area, matched only by strip or ribbon form. The design methodology for wire actuator is documented in Tom Waram's *Actuator Design Using Shape Memory Alloys* [9]. His approach assumes a linear stress strain behavior of the alloy in the operational temperature range (Mf – Af). Another assumption is that the given design parameters are only force and stroke. The actuator force and diameter are related by the stress:

$$\sigma = \frac{F}{A_{cs}} \tag{2.1}$$

Where σ represents the maximum shear stress allowed and F the required operating force. The maximum stress value is related to the lifespan of the memory element or the number of cycles the actuator can perform. This parameter if chosen conservatively and can provide to hundreds of thousands of cycles. The designer can obtain an approximate value for the maximum high temperature shear stress from the manufacturer according to the desired life of the actuator.

For a wire, the cross sectional area becomes:

$$A_{cs} = \frac{\pi \cdot d^2}{4} \tag{2.2}$$

Substituting 2 into 1 and solving for the wire diameter (d) we have:

$$d = \sqrt{\frac{4 \cdot F}{\pi \cdot \sigma}} \tag{2.3}$$

The length of the wire is given by:

$$L = \frac{S}{\Delta\varepsilon} \tag{2.4}$$

Where S represents the stroke parameter and Δε is the difference in strain between the low and high operating temperatures:

$$\Delta\varepsilon = \varepsilon_l - \varepsilon_h \tag{2.5}$$

The low temperature strain is a selected value and as is the case for the high temperature stress also limits the amount of cycles before failure for the actuator. For Nitinol this value can be as high as 8% for a few cycles. A value of 5% will yield thousands of cycles before failure in the same alloy. It is important to keep in mind that these values

are dependant in the type of alloy implemented since using the same values in Ni-Ti-Cu for example would yield far less cycles. From Hooke's Law we can obtain the high temperature strain:

$$\varepsilon_h = \frac{\sigma_h}{E_h} \tag{2.6}$$

where Eh is the Young Modulus of the Material at the high temperature. The length increment of the wire at the high temperature becomes:

$$L_i = \varepsilon_h \cdot L \tag{2.7}$$

where Li is the length increment and L is the total length of the element. Using the Young Modulus definition once again but this time in the low temperature range and solving for the low temperature shear stress gives us:

$$\sigma_l = \varepsilon_l \cdot E_l \tag{2.8}$$

Assuming no two way training is present in the SMA element the total bias force required to revert the wire back to its martensitic un-twinned or deformed state can be described as follows:

$$F_r = \sigma_l \cdot A_{cs} \tag{2.9}$$

Strip or Ribbon Shape

A strip shape can provide the same amount of force per cross-sectional area as wire. Among the advantages of using this type of shape is the increased cross-sectional area, which translates to a higher force and a SMA strip can also replace a wire bundle making it more attractive when fastening. The main disadvantage of an increased area is the increased heating and cooling times, which would yield lower overall cycle rates for the element.

Calculation for this type of shape follows that of wire with the only difference being the element area:

$$A_{cs} = w \cdot h \tag{2.10}$$

The dimensions in the strip element are related by:

$$R_{w-h} = \frac{w}{h} \tag{2.11}$$

R_{w-h} represents the strip's width to height ratio. This number is restricted by the processing capabilities of the manufacturer with typical values ranging from 10 to 15. Ideally the maximum possible width-height ratio will yield the lowest height for the same area. The advantage to having small height relates to a high heat transfer rate between the SMA element and its environment. Another factor affected by the shape memory height is the minimum bend radius. When a SMA is bent the stresses at the surface area of the bent region will be higher than the rest of it. As a result the life of the element can be considerably reduced. Gilbertson [10] recommends the minimum bend radius for a wire to be:

$$r_{\min} = 50 \cdot d \tag{2.12}$$

In the previous equation d represents the wire diameter and r_{min} is the minimum bend radius. For strip this value is fifty times the height:

$$r_{\min} = 50 \cdot h \tag{2.13}$$

Designing for the lowest possible height, the strip area becomes:

$$A_{cs} = R_{w-h} \cdot h^2 \tag{2.14}$$

Substituting 2.14 into 2.1 and solving for h yields:

$$h = \sqrt{\frac{F}{\sigma \cdot R_{w-h}}} \tag{2.15}$$

Rearranging 2.11 we can calculate the width as follows:

$$w = R_{w-h} \cdot h \tag{2.16}$$

The rest of the calculations for strip follow equations 2.4 through 2.9.

Spring Shape

Shape memory springs offer an increased amount of stroke at the expense of a reduced actuation force. The increased stresses that develop in the wire when setting this form can also potentially reduce its life considerable. The methodology to calculate shape memory spring also follows Waram's [9, 11] procedure as outlined below.

Compression spring calculations

A compression shape memory alloy spring will behave as shown in Figure 2.1, where at low temperature the spring will be compressed and when heated will extend with a pushing actuation.

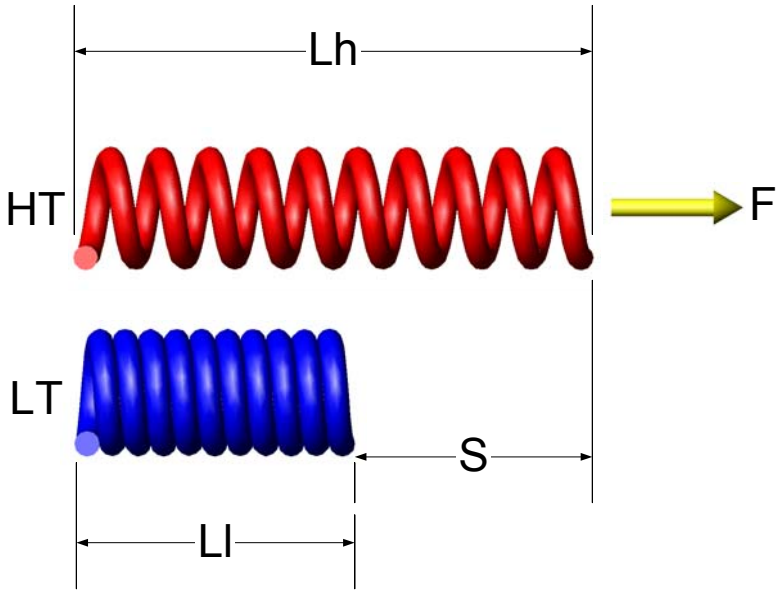

Figure 2.1 SMA compression spring actuation.

The expression for shear stress in a spring is described as:

$$\tau = \frac{8 \cdot F \cdot D}{\pi \cdot d^3} \cdot K = \frac{8 \cdot F}{\pi \cdot d^2} \cdot C \cdot K \qquad (2.17)^1$$

The value F represents the axial load applied, D is the average diameter of the spring, d represents the wire diameter, K the correction factor applied, and C is known as the spring index:

$$C = \frac{D}{d} \qquad (2.18)$$

With the exemption of the K factor, equation 2.17 is the torsional stress for a solid round bar. The K value, also know as Wahl correction factor, corrects this shear stress to account for transverse and torsional shear stresses present in a spring:

$$K_w = \frac{4 \cdot C - 1}{4 \cdot C - 4} + \frac{0.615}{C} \qquad (2.19)$$

Juvinall and Marshek [12] recommend the use of equation 2.19 for fatigue loading whereas equation 2.20 is often used for static loading only:

$$K_s = 1 + \frac{0.5}{C} \qquad (2.20)$$

Because of fatigue limitations in shape memory alloys the shear stress in 2.17 must be set by the designer to a value that would yield the desired life for the actuator[2]. From equation 2.17 we can obtain multiple wire diameters for the actuator for acceptable values of C ranging from 3 to 12:

---

[1] Equations 2.17 through 2.20 apply only to normal geometry springs: C>3, λ<12° (helix angle).

[2] The maximum shear stress depends heavily on the type of alloy used. Estimate values for 100,000 cycles for Ni-Ti and Ni-Ti-Cu are 170 Mpa and 140 Mpa respectively.

$$d = \sqrt{\frac{8 \cdot F \cdot C \cdot K}{\pi \cdot \tau}} \tag{2.21}$$

There are two factors that relate to the value of C in the design specifications: the cycle rate and the envelope volume of the actuator. Since the cycle rate is a function of the wire diameter, a value of C can be selected to accommodate a desired cycle rate. Shape memory alloy manufacturers usually provide actuation timetables for different wire diameters as shown in Table 2.1.

Table 2.1 Actuation times for various sizes of Flexinol wires in still air [11].

Name	Flexinol 025	Flexinol 050	Flexinol 100	Flexinol 150	Flexinol 250
Diameter (μm)	25	50	100	150	250
Max. Contraction Speed (sec)	0.1	0.1	0.1	0.1	0.1
Relaxation Speed (sec)	0.1	0.3	0.8	2	5.5
Typical Cycle Rate	55	46	33	20	9

The other method for setting the C value depends on the envelope volume of the actuator that depends on the spring outer diameter and length, which will be discussed next.

The average diameter of the spring can be obtained from 2.18 solving for D:

$$D = c \cdot d \tag{2.22}$$

The outer and inner diameters can be obtained from equations 2.23 and 2.24:

$$OD = D + d \tag{2.23}$$

$$ID = D - d \tag{2.24}$$

The number of turns in the spring can be obtained from:

$$n = \frac{d \cdot S}{\pi \cdot D^2 \cdot \Delta\gamma} = \frac{S}{\pi \cdot D \cdot C \cdot \Delta\gamma} \tag{2.25}$$

Where S represents the stroke of the actuator, and $\Delta\gamma$ the strain difference at high and low temperatures:

$$\Delta\gamma = \gamma_l - \gamma_h \tag{2.26}$$

The low temperature shear strain also affects the overall life of the actuator and must be set to a reasonable value. The high temperature shear strain can be obtained from the stress strain material chart for the assumed high temperature shear stress. Another method for estimating this value is by assuming a linear stress-strain behavior in which case the high temperature shear strain can be evaluated from the high temperature shear stress, τ_h and shear modulus, G_h:

$$\gamma_h = \frac{\tau_h}{G_h} \tag{2.27}$$

The spring rate for the high and low temperature ranges can be evaluated as follows:

$$k_h = \frac{G_h \cdot d^4}{8 \cdot n \cdot D^3} = \frac{G_h \cdot d}{8 \cdot n \cdot C^3} \tag{2.28}$$

$$k_l = \frac{G_l \cdot d^4}{8 \cdot n \cdot D^3} = \frac{G_l \cdot d}{8 \cdot n \cdot C^3} \tag{2.29}$$

With the spring rate we can evaluate the high temperature spring deflection as:

$$\delta_h = \frac{F}{k_h} \tag{2.30}$$

Since the stroke is the difference between the low and high temperature spring deflections we can derive the low temperature deflection from that as follows:

$$\delta_l = S + \delta_h \tag{2.31}$$

At low temperature the spring will be compressed with a length described by:

$$L_l = d \cdot (n + 3) \tag{2.32}$$

At the high temperature the spring will actuate to a length of:

$$L_h = L_l + S \tag{2.33}$$

The free length of the spring will be:

$$L_f = L_h + \delta_h \tag{2.34}$$

For one-way memory springs the required force to revert the shape memory alloy to its deformed martensite is given as:

$$F_r = k_l \cdot \delta_l \tag{2.35}$$

The envelope volume of the spring can be evaluated from the occupied area and height:

$$A_e = \frac{\pi \cdot OD^2}{4} \tag{2.36}$$

$$V_e = \frac{\pi \cdot OD^2}{4} \cdot L_f \tag{2.37}$$

If designing for an effective envelope volume an iteration process is recommended at this point to evaluate the best value for the spring index.

Extension spring calculations

A SMA extension spring will behave as shown in Figure 2.2. At the low temperature the spring will be extended and when heated will contract providing a pulling force.

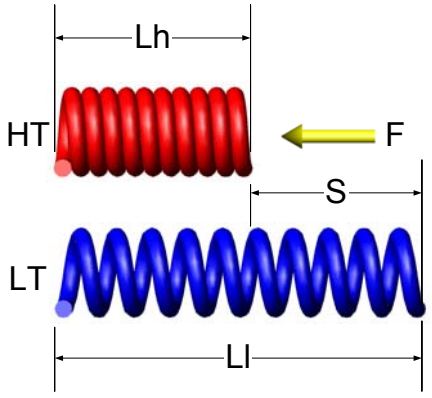

Figure 2.2 SMA extension spring actuation.

With the exception of the spring lengths the equations from the previous section can be used to determine the spring diameters, number of turns, spring rates and reset force. Since the actuation for a spring working in extension is reversed from that in compression the lengths must be reevaluated. The spring body length describes a fully compressed spring:

$$L_b = d \cdot (n+1) \tag{2.38}$$

Where n is the number of turns of the spring. The free length of the spring or the length at which the shape setting takes place can now be evaluated as a function of the body length:

$$L_f = L_b + 2 \cdot ID \tag{2.39}$$

When heated the spring will have a length of:

$$L_h = L_f + \delta_h \tag{2.40}$$

Since the stroke must be equal to the difference of the high and low temperature lengths the low temperature length can be calculated as:

$$L_l = L_h + S \tag{2.41}$$

where S is the stroke.

Shape memory alloy spring design calculator

During the course of this research a spring actuator was considered as one of the possible final prototypes. For this endeavor an applet was created to help in calculating the design characteristics of SMA springs. Figure 2.3 shows a screenshot of the applet, which can be found at http://plaza.ufl.edu/jrsan/smad-main.htm. The java based applet takes as input all the variables found in the spring calculations shown on the previous sections and outputs a 3D rendered model of the spring the user has the ability to view

the free, low, and high temperature lengths for the spring. Appendix A provides the java code used for the applet as well as additional code for the 3D primitives.

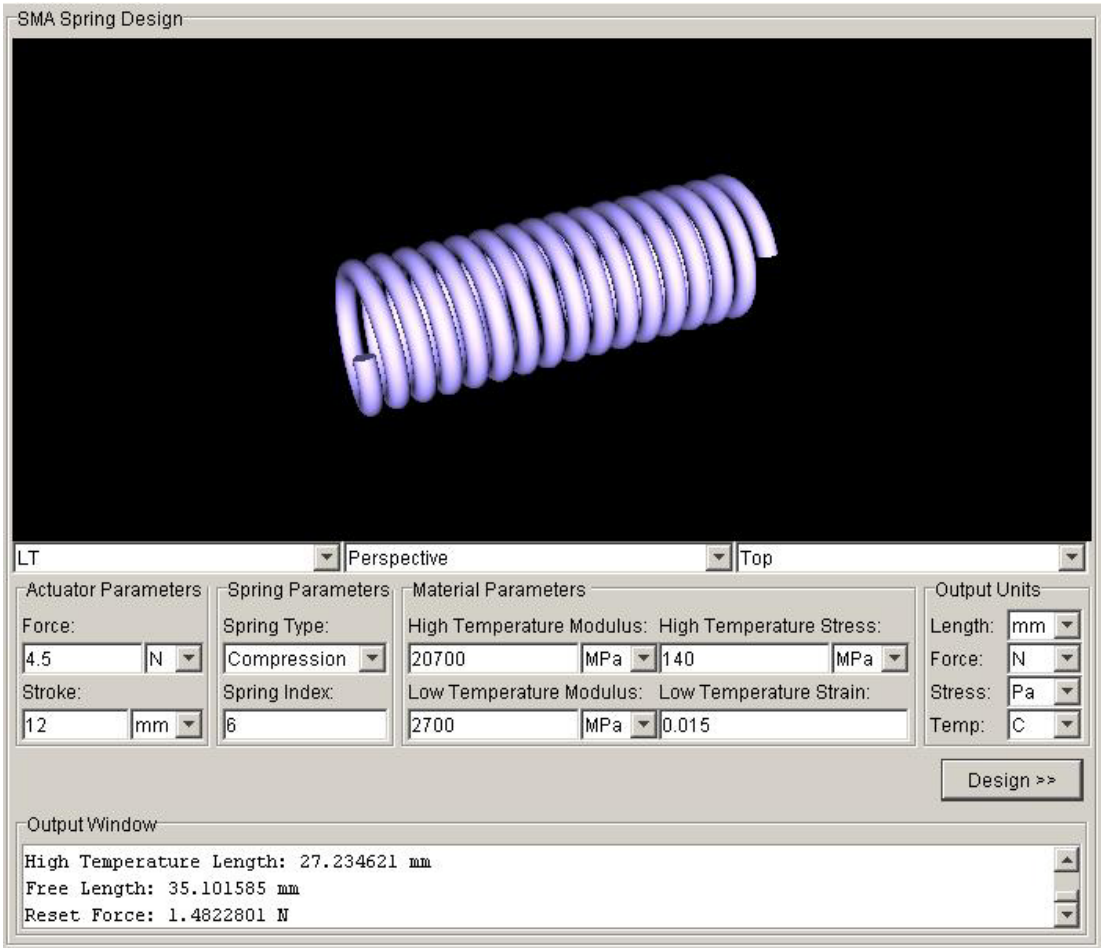

Figure 2.3 Shape Memory Spring Design Calculator.

Special Forms

Even though the most popular forms for shape setting are wire and spring there are however additional shapes that have been used successfully in many designs. Among the most popular of these are cantilever beam, shape memory tubing, and recently shape memory stents have also been added to the list.

Cantilever beams in its many iterations fall in the middle of the road when force and stroke are concerned. The force output, although not as high as for straight wire or

ribbon, is not as low as for spring design. On the other hand its stroke even though is not as high as for a spring design is not as small as for a straight wire element.

Shape memory tubing elements shrink when heated thus providing a clamping force that can go as high as 5000 lbf. This type of shape has been used successfully in shaft collars and release mechanisms, all of which are current available commercial products.

Shape memory stents are being developed at Sma-Inc for medical applications. Among its main features is the biocompatibility of the shape memory material, Ni-Ti, and their ability to expand. Stents are currently being used as implants for angioplasty procedures.

Activation Methods

Electrical Activation

Because of their metallurgical composition shape memory alloys possess an inherently high resistivity (especially Ni-Ti), which means they can be heated and subsequently activated by passing a direct current through them. The resistance can be evaluated as a function of their length and cross-sectional area a follows:

$$R = \frac{\rho \cdot L}{A} \tag{2.42}$$

Where ρ equals the SMA resistivity, L is the free length of the element, and A its cross-sectional area. From Ohm's Law we can calculate the voltage required for activation as:

$$V = I \cdot R \tag{2.43}$$

The power requirement can be evaluated as:

$$W = I \cdot V = I^2 \cdot R \tag{2.45}$$

The current value can be empirically evaluated for the specific ambient conditions on which the actuator must operate. Some companies do offer recommended current values for their alloys but most of them are only suited for their most popular wire shapes and usually at ambient temperature and still air conditions.

Waram presents a more precise method for estimating the current value, and activation and cooling times [9]. The formulas used were derived from testing on a specific type of alloy under still and forced air conditions. Since the thermo-mechanical properties of shape memory materials vary greatly from alloy to alloy it is best recommended to evaluate the activation current by means of testing.

Thermal Activation

Since shape memory activation is temperature dependant thermal actuation is also possible. The idea is to control the medium on which the SMA lies and adjust its temperature between martensite and austenite temperatures. This, however it is easier said than done. The control challenges associated with this type of activation far outweigh its benefits. The main problem for this type of activation lies in the operating temperature range, which has a typical value of 70° C between the martensite and austenite finish temperatures. This high value is in part due to the temperature hysteresis present in the alloy. The added challenge for the designer comes in the form of building a heat exchanger that will be able to heat and cool the SMA and in the process a method to precisely control the chamber temperature for position control. The shape memory effects usually associated with thermal actuation are two-way and R-transition the latter because of its low temperature hysteresis.

SMA Actuator Technologies

The inherently high power vs. weight ratio that exists in shape memory alloys makes them ideally suitable for work producing devices. These actuators can be categorized in two major groups: linear and rotational. Subsequently each one of these groups can operate as a differential or non-differential actuator. SMA actuators can also be categorized as high stroke or strain actuators, high force actuators, or both. The bulk of the work though has been in overcoming the maximum displacement possible for any shape memory alloy configuration. Since shape memory alloys are by nature powerful the main limitation has been the useful stroke that can be derived from them. The following sections will show different kinds of SMA actuators that have been developed.

Rotational actuators

The most popular form for this type of actuator for position control employs a shape memory wire with one end attached to ground and the other connected to the side of a rotational joint. As the wire contracts the joint rotates in one direction. This type of mechanism can be of single or differential actuation. In single actuation the joint rotates by using only one shape memory element and on the other side a bias spring provides the resetting actuation for the SMA. This type of actuator has been used in Hitachi's robot hand [13]. The differential version of the rotary actuator replaces the bias spring with an additional SMA element making the actuator act in an antagonistic fashion. One of the limitations with this kind of design is that no continuous rotational motion is achievable and the range of rotation is usually less than 180 degrees. Some of the other limitations, which are inherent in all shape memory actuators, have to deal with the response times. Gorbet and Russell [14] address this issue by implementing a heat sink in a differential rotational actuator as shown in Figure 2.4. As one of the wires activates the heat sink

setup rotates and is placed in contact with the other wire, which is now being cooled down.

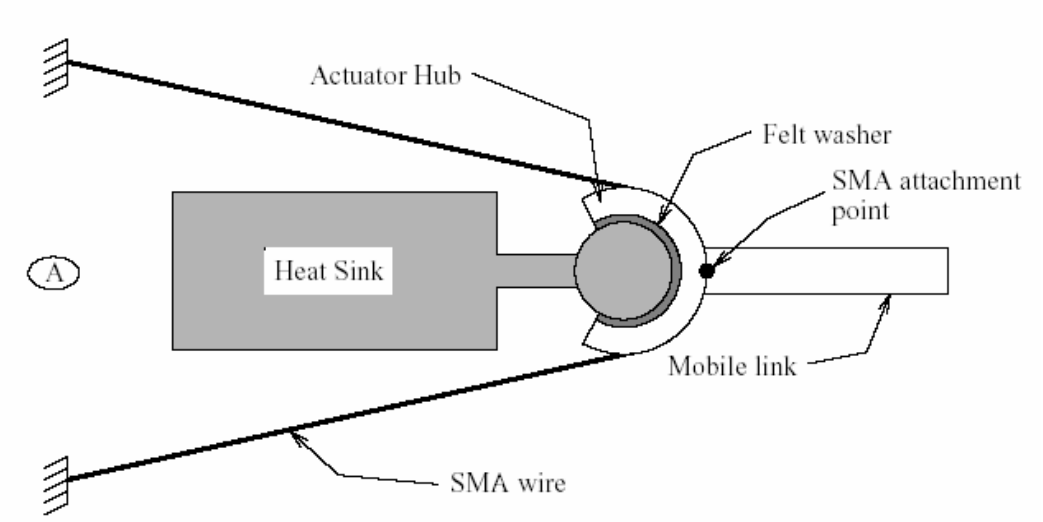

Figure 2.4 Schematic Gorbet and Russell Differential Actuator [14].

Linear actuators

Due to the nature of shape memory alloys they are most efficient when implemented in a straight fashion. The major drawback that this type of implementation presents is a maximum achievable strain of only 8% of the actuator's length for a mere few cycles before rendering the element useless.

Several studies have focused their attention on improving the stroke restriction. The most compact way of improving the stroke is by setting the shape of the SMA to a spring form. This provides an increased stroke at the cost of force due mainly to the transverse shear and curvature effects in the spring. A very good method to follow in spring design is provided by Tom Waram [9] and outlined in an earlier section of this review.

Another design to overcome strain restrictions was developed by Grant and Hayward [15]. The design involved the use of notched disks on which the shape memory

element would be wound, but instead of positioning the wires in a straight fashion the placement was made at angles as shown in Figure 2.5. The design was modular meaning that cells could be stacked one on top of each other for increased stroke. On his prototype Grant used one-way shape memory alloy and a compression spring was implemented through the center of the mechanism to provide the bias force required to reset the martensite. By increasing the number of notches on the disks augments the force of the actuator without having to increase the diameter of the wire elements. The result of their investigation was a compact (17 mm D x 30 mm L), lightweight (6 grams) actuator capable of producing 4 N of force and a stroke of 2.5 mm.

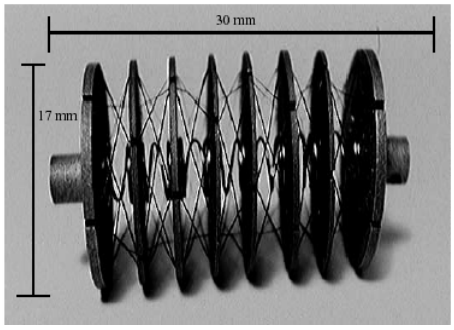

Figure 2.5 Grant and Hayward High Strain SMA Actuator [15].

Other designs implement the use of pulleys to route the wire. The main focus of this implementation is to reduce the amount of energy needed for actuation while preserving a high force. When compared to a straight wire the pulley method will provide a higher force with a lower power requirement. Another advantage of using this type of arrangement has to deal with the compact packaging of the shape memory elements, which is always one of the main reasons when designing applications with SMA's in mind. An example of this implementation was developed by Soares, Brash and Grow [16] in their SMA Artificial Hand. Their design used two sets of pulleys, one on each side of the actuator to route a SMA wire bundle. The total displacement achieved

was 7.2 mm on a package with a length of 95 mm using 263.5 mm long wires while providing a force of 27 N. The wire bundle helps reduce the response times of the actuator by providing a lower per element cross sectional area. Mosley and Mavroidis [17] also used the wire bundle setup but this time the arrangement was in a straight fashion. The final actuator was able to lift a total mass of 100 lbs. Here again a wire bundle was implemented to reduce the response times of the actuator. This was especially important since the intention of the researchers was to study the viability of SMA actuator technology for robotic applications. Although they did not address the issue of limited stroke they did outline a way of obtaining large angular deflections by sacrificing part of the available force from the actuator in a reciprocating fashion. The wires, 48 in total, were Flexinol 150, 12 in long and provided a stroke of 0.5 in. One important aspect of their research was the implementation of the current-voltage required to drive the wires. Instead of bundling the wires in parallel, which would result in a high current, the use of a combination of series and parallel connections between the wires was used. Making the mechanical connection in parallel and segmenting the bundle into groups for electrical connection in series allowed them to reduce the activation current. In the experimental phase of their design the researchers found in some instances a chaotic behavior of the SMA [17].

Theory vs. Empirical Implementations

As with most occurrences in nature the behavior of shape memory is not entirely dictated by theory. Although great effort has been placed into developing a mathematical model for shape memory behavior for the most part the desired outcome always departs from the formulas. Although the work of Waram, Wayman, and Duerig help in terms of providing up to some extent a theoretical base to shape memory design the fact remains

that the actual real life results will vary in some form. The main reason can be attributed to the manufacturing and production of shape memory alloys since no two batches of material will ever be the same. This becomes much more important considering that a change in chemical composition of less than one percent in the alloys will produce dramatic changes in the mechanical and thermal properties of the resulting material. Some companies like Sma-Inc in California are implementing some quality control standards, like ISO-9002, to aid in maintaining uniformity among their shape memory alloy product line and even then each material will behave different. The best method for designing with shape memory alloys is by empirical implementation and testing of the material itself. Shape memory distributors do provide customers with datasheets that actually prove more useful and accurate than trying to design using theoretical formulas. Besides obtaining the properties for the material from the manufacturer the reader is also encouraged to do their own testing for more accurate results. Another factor to consider is that the material itself will change its technical characteristics over a period of time when implemented. The changes may be subtle like acquiring some two-way memory in the form of "walking" or obvious like a change in length and maximum strain when subjected to higher currents than the ones the material will allow. All in all the designing of shape memory requires a great amount of knowledge on the part of the designer to account for these potential problems and oversee others.

CHAPTER 3
PROTOTYPE DESIGN

Over the course of this research many designs for shape memory actuators were considered and finally one of them was implemented. The main goal of this investigation was to explore shape memory technologies and its viability for control applications. Several actuators were designed taking into consideration stroke and force limitations. This chapter will focus on these designs.

Preliminary Considerations

Although shape memory alloys can take almost any form possible, this investigation limited the form of the SMA elements to commercially available alloys and shapes. This greatly limited the scope in terms of the kind of alloys and their shapes to only a few choices. Although this may seem to hinder the objectivity of the research by taking this approach a more viable solution may be implemented in the end. Another factor to consider is that prototyping of shape memory materials to posses certain shape and mechanical properties is an expensive endeavor, which eventually would result in a cost ineffective solution.

Large Force Shape Memory Alloy Linear Actuator

The main goal for this actuator was to implement shape memory alloy as the driving mechanism for a linear actuator. The force is kept large while the displacement is minimal. The design would take advantage of straight shape memory alloy wires to produce large amounts of force. The following sections provide the main parameters considered in the design.

Shape

Among the shapes considered for this type of design where wire and ribbon form straight annealed and helical form. As discussed in Chapter 2 of this work each of these forms have their advantages and disadvantages. Essentially a wire or ribbon is more efficient than a coil form since there is no loss of force due to traverse and torsional shear. On the other hand the spring shape provides a higher displacement when compared to straight annealed elements. Taking into consideration the large force requirement the selected shape was set to be straight annealed, thus leaving two more options to be considered: wire or ribbon.

Cycle Rate

For this work a cycle is defined as the amount of time needed to actuate and relax a shape memory element and the cycle rate as the amount of cycles the actuator can perform per unit of time. The cycle time can be divided into two: heating or actuation time and relaxation or cooling time. Since actuation is done electrically most elements will actuate in less than one second. For ribbon and wire forms under the same environmental conditions the cooling time will depend for the most part on the cross sectional and surface areas of the element in question. Ideally a flat ribbon shape with a high width to height ratio should provide more surface area than a wire with the same cross sectional area and faster cooling times. However for availability reasons a wire form was selected for this endeavor. Since the final design implements straight annealed elements, wire and ribbon actuators can be used interchangeably if ribbon material is available in the future.

Geometrical and Power Considerations within Cycle Rate

Having selected a wire form as the main element, attention focuses on the wire diameter itself. Keeping in mind that the final design will implement commercially available materials information was gathered for different sizes of shape memory alloy wires and their technical data especially those concerning the activation and cooling times. Dynalloy, a California based shape memory alloy manufacturer, offers a line of shape memory alloy wires named Flexinol. Mainly Flexinol products come in two categories HT, which stands for High Temperature and LT, which stands for Low Temperature. The LT alloys have an Af (Austenite Finish Temperature) of 70°C whereas the HT alloys posses an Af temperature of 90°C. Table 3.1 presents the Flexinol product line with their respective contraction and off times.

Table 3.1 Technical characteristics of Flexinol wires. Taken from www.dynalloy.com .

Diameter Size (Inches)	Resistance (Ohms/Inch)	Maximum Pull Force (gms.)	Approximate* Current at Room Temperature (mA)	Contraction* Time (seconds)	Off Time 70° C Wire** (seconds)	Off Time 90° C Wire** (seconds)
0.0015	21.0	17	30	1	0.25	0.09
0.002	12.0	35	50	1	0.3	0.1
0.003	5.0	80	100	1	0.5	0.2
0.004	3.0	150	180	1	0.8	0.4
0.005	1.8	230	250	1	1.6	0.9
0.006	1.3	330	400	1	2.0	1.2
0.008	0.8	590	610	1	3.5	2.2
0.010	0.5	930	1000	1	5.5	3.5
0.012	0.33	1250	1750	1	8.0	6.0
0.015	0.2	2000	2750	1	13.0	10.0

Table 3.1 also presents recommended values for maximum pull force and an approximate current value for activation. We can determine the most efficient wire diameter by analyzing the required current values for a constant load and varying the number of wires in parallel needed to achieve such load. Taking the largest possible load

capacity to be 2000 gms and assuming one inch in length wires the power requirement can be calculated.

Table 3.2 Electrical Characteristics of Flexinol by Diameter.

Wire Diameter (in)	No. Of Wires	Resistance (Ohms)	Current (mA)	Power (Watts)	
0.0015	117.65	21	30	2.223529	←Max
0.002	57.14	12	50	1.714286	
0.003	25.00	5	100	1.250000	
0.004	13.33	3	180	1.296000	
0.005	8.70	1.8	250	0.978261	←Min
0.006	6.06	1.3	400	1.260606	
0.008	3.39	0.8	610	1.009085	
0.010	2.15	0.5	1000	1.075269	
0.012	1.60	0.33	1750	1.617000	
0.015	1.00	0.2	2750	1.512500	

Table 3.2 gives the most and less efficient wire configurations. A bundle of approximately 9 0.005 in diameter wires will provide the same force for approximately 56% less power than using a bundle of 117 0.0015 in wires. This value will require that any wire other than the 0.015 in be configured in a bundle. When comparing the power requirements for 0.008 in and 0.005 in wires the advantage of using the latter is only 1.38% but the amount of wires is reduced by almost 5. This becomes especially important when considering that as the number of wires in the bundle increases so it does the complexity of the actuator and the number of challenges the designer must face. To reduce the number of wires in the bundle while keeping a high efficiency a Flexinol 0.008 in wire was selected.

Load

Due to the low achievable strains that a SMA element can provide the bulk of the actuators designed that employ this technology are being implemented towards micro-scale applications. Although they do provide a high force for a micro-scale application

the actual load pales when compared to the macro application loads. To put the loading parameter in context we must first consider micro-scale loading. Take for example one of the most popular shape memory alloy actuators: the SMA piston shown in figure 3.1.

Figure 3.1 Shape Memory Alloy Piston.

This actuator implements a shape memory alloy spring working in tension to provide a force of up to 1 lb over a functional maximum stroke of 1 in. Because it is a spring, the space is preserved while trading off actuation cycles, which are lower due to traversal and torsional shear stresses. This device can be though out to be a large force SMA actuator for micro-scale applications whereas the force is small for macro applications. Multiplying this value a hundred times will yield a more suitable value for macro applications. Although this would be an arbitrary value a 100 lbs is more than enough number to claim the actuator as suitable for macro applications in the loading realm. Shape memory alloy actuators that have been developed in the past as claiming to be large force posses loading values of up to 20 pounds; this would mean that an actuator with 5 times the capacity of this one would also fit this description.

Stroke

Although the purpose of the actuator to be designed is only for large force, the stroke must posses a reasonable value that would give some room for the implementation of control. Too small of a stroke would make the actuator virtually impossible to control since small increments in current transform to big movements. Another factor that dominates this parameter is the hysteresis associated with the shape memory element. Since the actuation temperatures (As to Af) are different than the cooling ones (Ms to Mf) this makes the modulation range of the actuator a higher value than with purely linear systems. Overall a value of 1 in was selected having the actuator work on average between 4 to 5 percent strain thus ensuring hundreds of thousands of cycles.

Mechanical Hardware

Based on the selected shape memory elements a linear actuator was designed and implemented. The following is the design criteria used for the resulting actuator:

1. A parallel configuration will account for the smaller, faster elements while providing a large force when working together.
2. Serviceability must be kept manageable.
3. Versatility will allow interchanging the shape memory alloy elements for other wires and thus serving as a testing platform for current and upcoming shape memory alloy wire and ribbon technologies.
4. Reset and tensioning devices must be implemented to ensure that no loss stroke is wasted and to allow for faster response. The reset mechanism will also provide a bias force so that the actuator is always ready to be activated.
5. Electrical connections must enforce that a uniform current passes through each wire.

The following section will discuss these points in more detail while observing the preliminary and final design implementations.

Wire array bundle:

The implementation of an array bundle provides a simple solution to multiple problems. When correctly implemented an array configuration must address the following:

1. The array must be able to maintain a uniform tension across all the wires.
2. The configuration must ensure that uniform current flows through all the elements in the array.
3. A parallel array should provide for lower response times by implementing faster elements.

The main purpose for the use of an array is to provide faster actuation while maintaining a large uniform force. The reasoning behind this is rather simple, actuation times is directly proportional to the cross sectional area of the wire. Higher cross sectional areas yield a higher actuation force per wire with the included drawback of slower cooling times. Since the scope of this work is the study of SMA in respect to actuator technologies, the response of the actuator is an essential parameter. The selected wire has a diameter of 0.008", which can sustain a load of 590 gms. The total force can be expressed as follows:

$$F_{TOT} = F_{BIAS} + F_{NET} \qquad 3.1$$

where F_{bias} is the reset force required to bring the actuator to its martensite state and F_{net} represents the total net force the actuator can provide. Although the reset force can be calculated by using the formulas described in Chapter 2 of this work the recommended values provided by the SMA manufacturers can be used to obtain an approximate value. This recommended value is 2/5 of the total load:

$$F_{BIAS} = \frac{2}{5} F_{TOT} \qquad 3.2$$

This value, however, is an approximated figure and it is assuming that the wires exhibit one-way memory effect. Testing on the wires indicates that they do exhibit up to some extent characteristics of two-way memory. This is an important finding since the net load that the actuator can be subjected to can be dramatically increased if the bias force is reduced. For the preliminary calculations the recommended value will be used which will later be address with more detail in the discussion of the bias load. As discussed earlier our target force for actuation is 100 lbs hence:

$$F_{NET} = 100 \cdot lbs \tag{3.3}$$

Substituting equations 3.2 and 3.3 into 3.1 we have:

$$F_{TOT} = \frac{2}{5} F_{TOT} + 100 \tag{3.4}$$

Solving for the total force we have:

$$F_{TOT} \cong 167 \cdot lbs$$

One 0.008" wire can pull 590 gms or 1.3 lbs, thus dividing the total force by the force that one wire can provide would yield the required number of wires:

$$N = \frac{F_{TOT}}{F_{WIRE}} = \frac{167}{1.3} \cong 128 \cdot wires \tag{3.5}$$

According to this figure a total of 128 wires would be needed to account for a 100-pound load. This value will gives us some kind of approximate number to be worked upon in the selection of the biasing mechanism discussed next.

Bias force

As mentioned in chapter 2 the bias force in the actuator would act as the reset mechanism to revert the actuator to its untwinned martensite state. The bias force can also be used, up to some extent, as a tensioning mechanism but it is recommended to

implement some kind of additional dedicated device for this endeavor that would account for small adjustments on the individual wires. The two most common mechanisms used to apply a bias force are a separate actuator in a differential fashion or the use of a spring, with the latter one being the most widely accepted. The final prototype implemented the spring technique to achieve the required untwinned martensite in the wires. Preliminary designs used the implementation depicted in Figure 3.2, that used linear ball bearing splines to maintain linear motion and encased in the shaft a compression spring to provide the force.

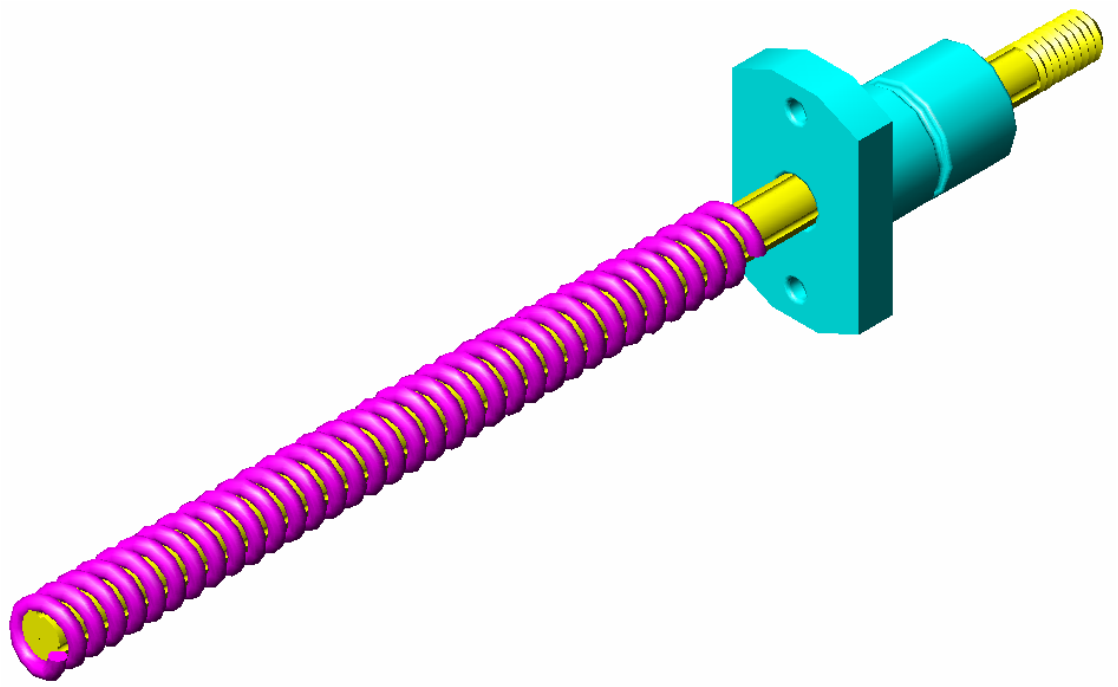

Figure 3.2 Initial Bias Force Mechanism.

The previous design was later discarded for a more favored approach that employs gas springs that would act twofold: to provide both the linear motion and the bias force. The gas springs also posses a more uniform spring rate than conventional music wire springs. The initial implementation of the gas springs used a pair of Stabilus Lift-O-Mat as shown in Figure 3.3.

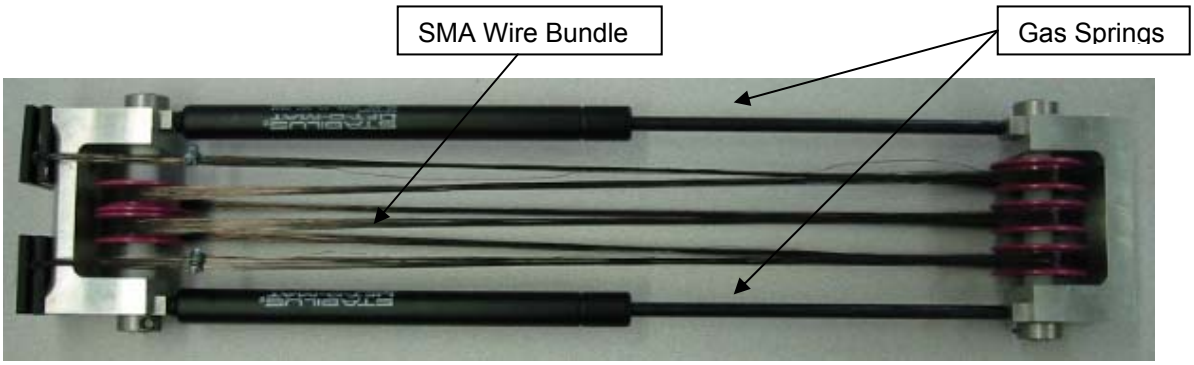

Figure 3.3 Initial Implementation of Gas Springs as Bias Mechanism

These springs had a total length of 11.5 in and a maximum load capacity of 33 lbs each, thus fulfilling the requirement for a bias force of 66 lbs. As previously discussed the shape memory wires did in fact exhibit two-way memory behavior. More accurately the wires, as they began to be actuated experienced walking, which is a form of shape memory behavior. If the wires did in fact experience some form of two-way memory then the requirement of the bias force could then be lowered which would result in an increase of the total net force. Having considered this a design decision was made to lower the load of the springs to 22.5 lbs each, which was the next available gas spring. This would result in a more efficient actuator with fewer wires.

Bundling technique

Initially a pulley design was implemented as shown in Figure 3.3. The main purpose of this configuration was to provide uniform tension across the wires and to supply an easy installation of the wires. The preferred method for mounting the wires was by bundling them prior to attaching them in the actuator. Although the wires were pre-bundled and tensioned, when mounted in the device some of them were looser than others (Figure 3.4). It was later concluded that the non-uniform tension across the wire bundle was due to the pulley system implemented. In some instances a wire would run though the inside of one pulley and later that same wire would run on the outermost part

of another pulley. This would result in some wires having a shorter length than others. Another factor that made this configuration unusable was due to the electrical connections to the wires. At any given run some wires would activate while others would remain without a current supply. The reason behind this phenomenon has to do with the conduction between wires. Although the wires have a layer of titanium oxide it is not sufficient to provide a practical insulation. As a result current would flow from one wire to another having in the end sections of wires not activated. A test was made using 26 0.015" diameter wires and the results were not encouraging. The test provided random results in the actuation of the wires. In some instances out of the 26 only 11 wires would be actuated while in other cases only 9 would be producing work and the number kept on changing. It was clear this design would not be achievable.

Figure 3.4 Initial Pulley design with loosed wires.

The previous failure resulted in the design and implementation of two plates each one having 104 drilled hole bed (Figure 3.5). All the holes were 2-56 drilled and tapped. Screws were used to provide for fixing each wire to the plates individually (Figure 3.6). The screws used were vented ones, which have a hole throughout its entire length. Figure 3.7 details the mounting of the wires through the hole bed plate and crimp. The wires were initially crimped on one side, then passed through one of the plates,

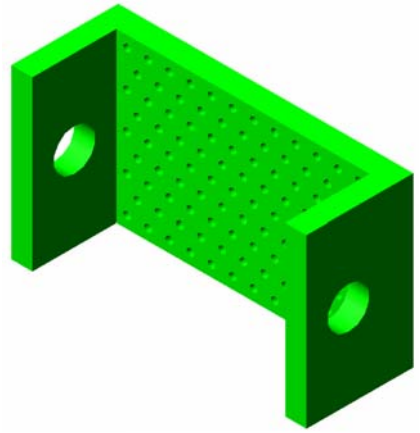

Figure 3.5 Hole Bed Plate.

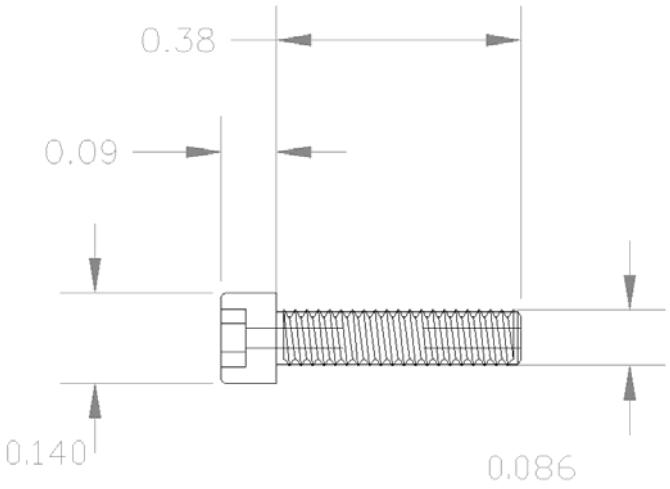

Figure 3.6 #2-56 Vented Screw. All units are in inches.

through the screw onto the other screw and plate at which point they were crimped on the other side. Besides providing for individual power connections to each wire, the design also provided for individual tensioning of the wires allowing for a more precise tuning of the actuator. Eventually this resulted in an added bonus since the wires can increase their length when actuated several times and although the change in length is minimal the individual tensioning design would ensure that the actuator is always ready to be actuated and that no loss in the available stroke occurs.

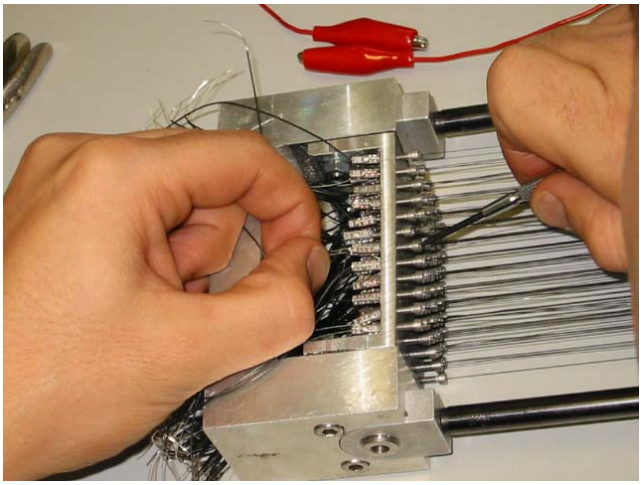

Figure 3.7 Mounting the wires into the plates.

Final prototype characteristics:

The final prototype complete with the test setup is shown in Figure 4.1. The actuator uses 104 SMA Flexinol elements working in parallel mode. Each one of the 104 wires is individually attached to the two hole plates (Figure 3.5) and fixed with the use of vented screws and crimps (Figure 3.7). The total force the wires can produce is:

$$F_{TOT} = N_{WIRES} \cdot F_{WIRE} = 104 \cdot 1.3 \cdot lbs = 135.27 \cdot lbs \qquad 3.6$$

Two Stabilus Lift-O-Mat nitrogen gas springs were implemented as the bias loading mechanism with a total length of 20 inches and a maximum pull force of 22.5 lbs each having a total bias load of 45 lbs. The total gravitational load that the actuator will be moving as part of the actuator itself is comprised of the sum of the weights for the bottom C-Bracket, two blade ends, 104 #2-56 screws, and the two body rods for the gas springs. This load comes to be approximately 3 lbs. The static force was calculated empirically to be approximately 15 lbs. From these parameters the default load that the actuator is subject to comes to be:

$$F_{DEFAULT} = F_G + F_S + F_{BIAS} = 3 + 15 + 45 = 63 \cdot lbs \qquad 3.7$$

From this value the net load for the actuator can be obtained to be:

$$F_{NET} = F_{TOT} - F_{DEFAULT} = 135.27 - 63 = 72.27 \cdot lbs \qquad 3.8$$

According to the manufacturers data sheet the wires in still air should contract with a recommended current of 610 mA for a total current of 63.44 A. The contraction time should be less than one second and the cooling or off time for relaxation should be at about 3.5 seconds this would give a total actuation cycle time of 4.5 seconds and a cycle rate of about 13 cycles per minute. The cycle rate can be increased by utilizing some form of active cooling on the wires like forced air and the effects of active cooling will be discussed in the next chapter.

CHAPTER 4
EXPERIMENTAL SETUP AND RESULTS

Test Platform

Hardware

Using a series of mechanical, control and software devices the actuator was tested. The frame was built using 80-20 structural aluminum, which would hold the linear actuator in place (Figure 4.1).

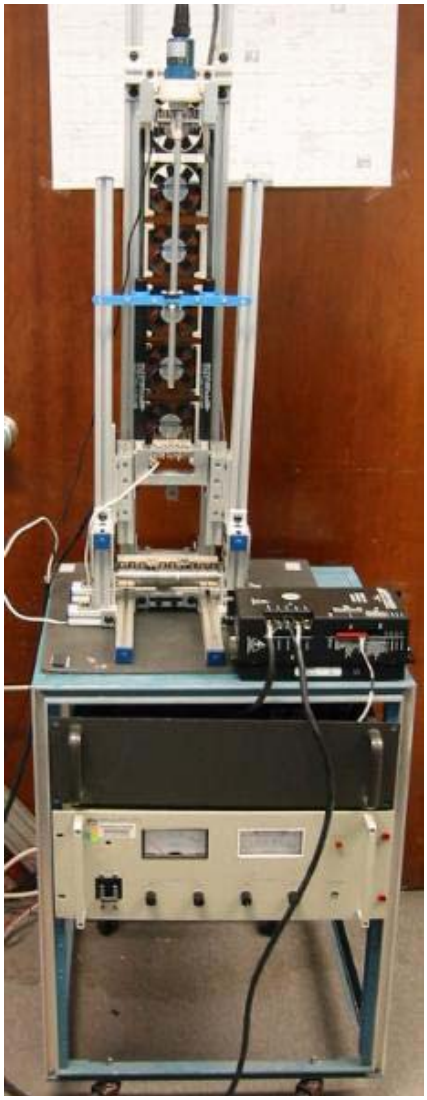
Figure 4.1 Final Prototype

The frame would also hold a tower of 12VDC 0.16A 19.W Brushless Radio Shack fans for cooling the shape memory alloy. Linear displacement was measured with the use of a Temposonics LDT encoder model TTSRCU0120 and power to the breakout box of the encoder was provided by a Lambda 18 V regulated power supply. Instead of using weights for the test mass a test load was designed using ten ConForce springs attached on its interior to a drum and on the other end to a plate as in Figure 4.2. This

provides for a small envelope test platform with a variable load from 0 to 100 lbs in increments of 10 lbs.

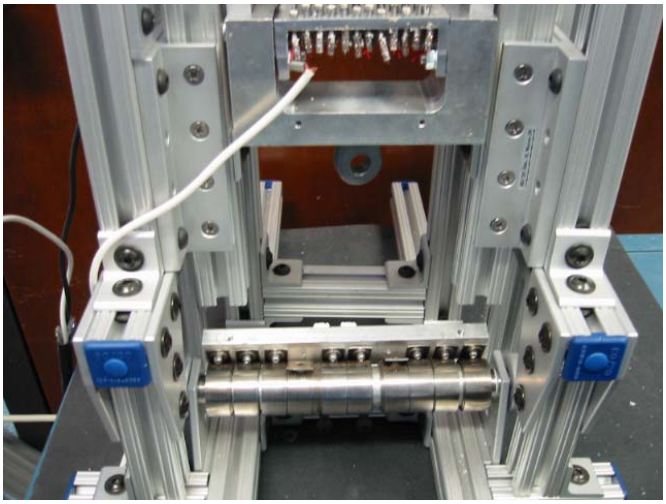

Figure 4.2 Conforce Springs Setup.

An HP MODEL 6268B DC Power Supply provided power for the actuator with a maximum current rating of 30 amps. A Systems in Motion Brush Type PWM Servo Amplifier model 120A10B unit was implemented in conjunction with the HP power supply to provide the current needed to actuate the wires. A Keithley Instruments digital/analog IO card attached to the PCI slot of a AMD Duron 750 MHz system with 256 MB of PC150 RAM was used to control the actuator in conjunction with LabView 5.1 software, which was utilized to model the Open, and Closed loop of the system.

Software

The use of Keithley Instruments IO card allows making use of a powerful program for data gathering and analysis called LabView. A data collection program was created using this software. The program was separated in three main areas: Device Status, Closed Loop Control and Open Loop Response. The device status portion of the UI allows the user to see and control manually the actuator by means of increasing the

reference voltage, turn on and off the cooling fans, see the current stroke as well as the filtered and unfiltered LDT signal and turn on or off the filtering of such signal.

The open loop transient response of the actuator allows the user to record the step response of the actuator. The user can also determine a delay time for recording, and off time until the recording to the data file stops to measure the cooling time of the actuator after the initial activation.

The open loop steady state response of the actuator recorded the response of the actuator to a given input, which is being incremented when no appreciable difference in stroke is observed. The run starts at Vref of 0V until 5V and can be incremented by a number, which can be set by the user. The user can also set the stroke threshold.

Finally the closed loop portion of the program implements a PID controller. In this segment of the program the user can set the PID constants namely: K_p, K_i and K_d, the loop's delay time and record to a file. The data is displayed visually in three charts and can be also recorded onto a file. The User Interface of the program is displayed in Figure 4.3.

The Tests

The open and closed loop response of the actuator under still air conditions was implemented for 104 0.008" Flexinol LT parallel configuration of wires.

Open Loop Response

Two types of open loop responses were taken: transient and steady state. The transient open loop response acquired data for a given step input and recorded time and stroke. The steady state response was time independent while reference voltage and stroke was recorded.

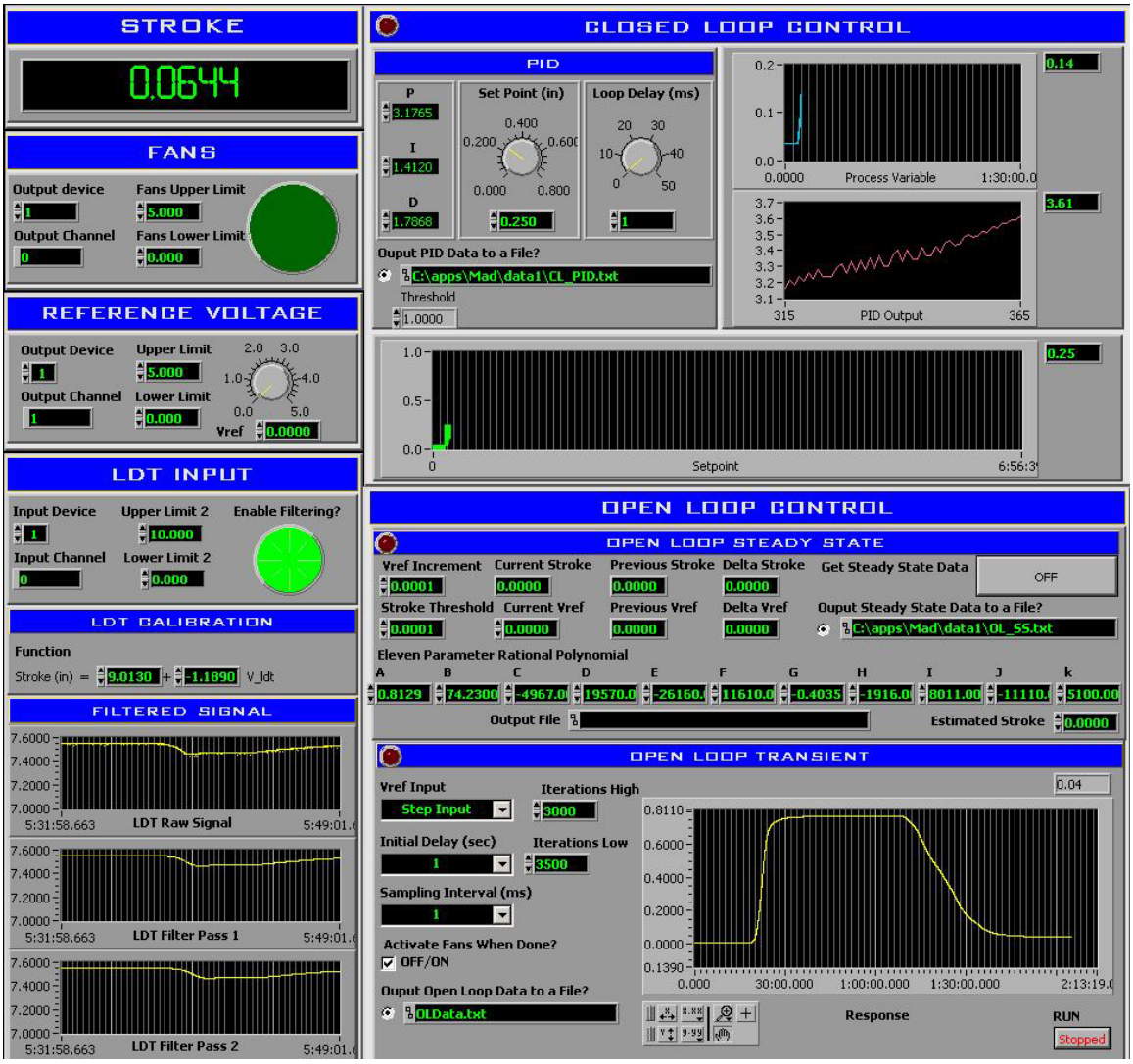

Figure 4.3 LabView Virtual Instruments for the SMA Actuator.

Transient open loop response

The response of the actuator was recorded for a given step input by setting the reference voltage to its maximum which is 5V. Data was collected for each of the three different loading conditions that the actuator was subjected to. Three runs were conducted for each of the three loads to calculate an average response. The response was recorded in a transient fashion. Since this is open loop this interface was also used to

obtain the response of the actuator for later calibration of the PID constants, which will be explained in the closed loop section of this chapter.

Testing for the 104-0.008" configuration under default loading, +40 lbs and +80 lbs were made. The three runs are compared in Figure 4.4

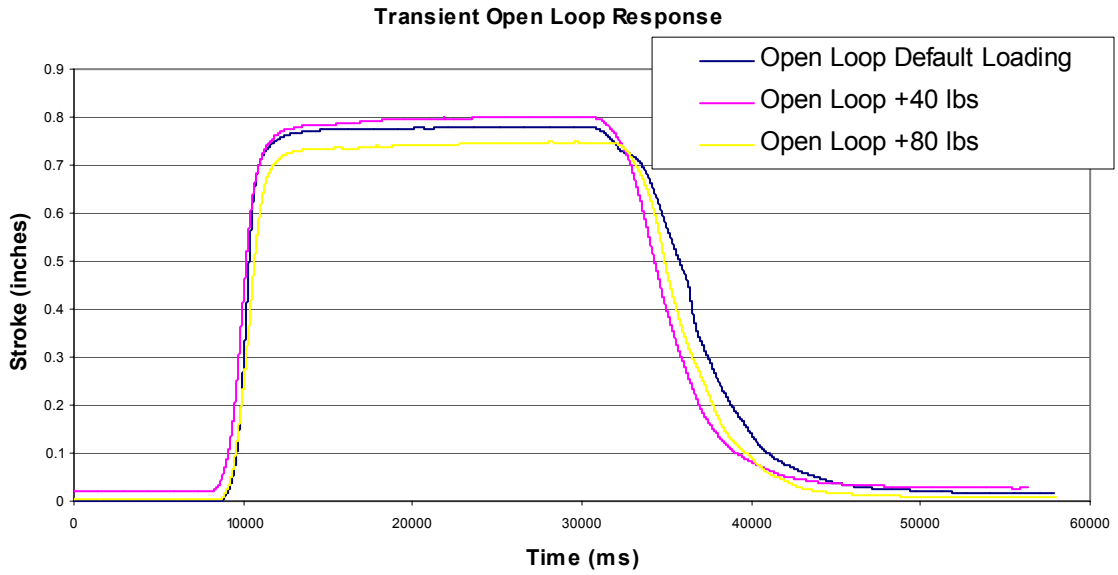

Figure 4.4 Transient Open Loop Response at all Loading Cases.

The maximum stroke for a step input was recorded to be 0.81" under default loading conditions while the lowest stroke was recorded for the +80 lbs loading case at 0.76". Overall the response of the actuator for a given step input remained practically unchanged regardless of the load that the actuator has to pull. This will prove to be important latter on when we discuss the calibration for closed loop control and the effects of proportional control on the actuator.

Open loop steady state response

Steady state data was collected for the 0.008" wires. The data collection software was programmed to collect the stroke transformed from the LDT voltage and compares

the current and previous values. If the difference exceeds a threshold set by the user then the voltage remains unchanged until the stroke has stabilized at which point time, reference voltage and stroke are recorded and the reference voltage increased by a unit set also by the user. Figure 4.5 show the response of such test.

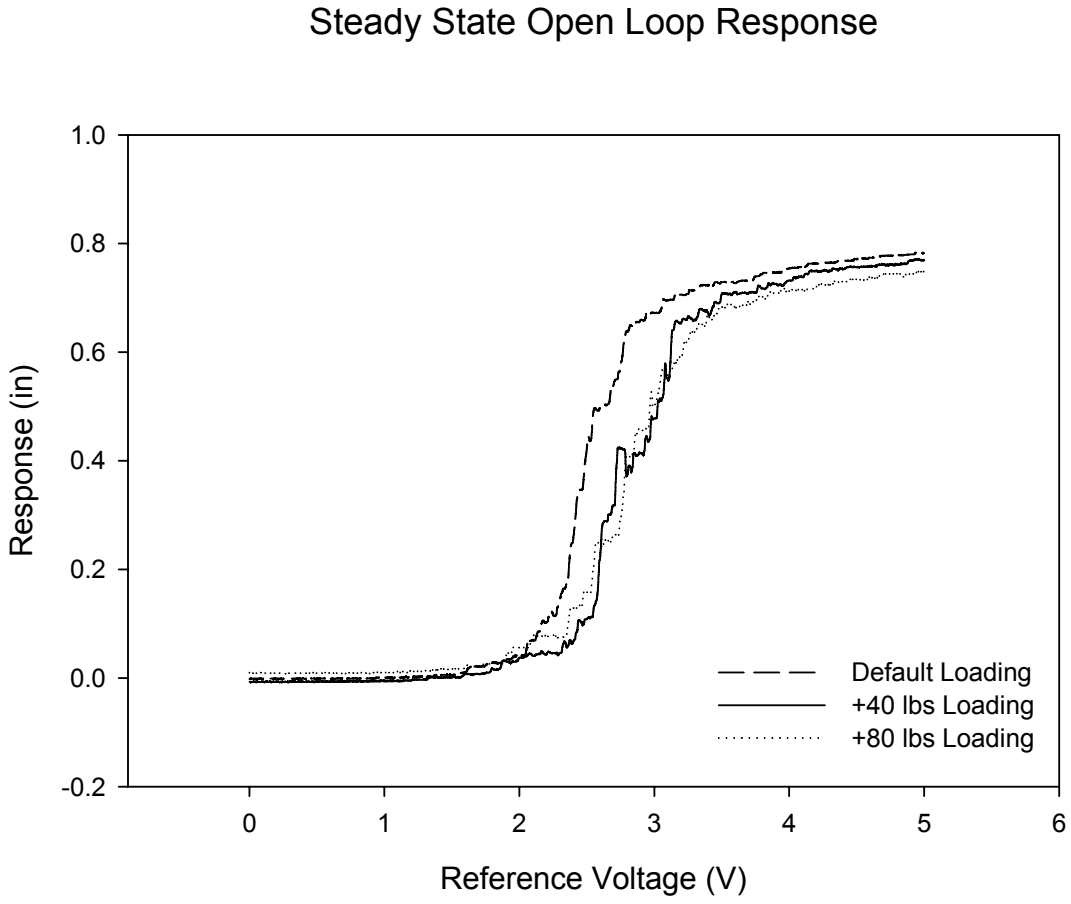

Figure 4.5 Steady state open loop response.

Closed Loop Response

Closed loop response was taken for different comparison standpoints. The first set of collected data was taken to illustrate performance of Nichols calibrated PID, PI and P controllers. Secondary data was collected in order to compare the Nichols calibrated PID to an optimized PID controller.

Overall closed loop response

Closed loop control was implemented for a PID, PI and P controllers. The controller is software based with the stroke as the input and the reference voltage as the output. The PID constants were obtained by using the Nichols tuning method [18]. For the calibration open loop response was plotted as shown in Figures 4.6 through 4.8 for the three different loading conditions.

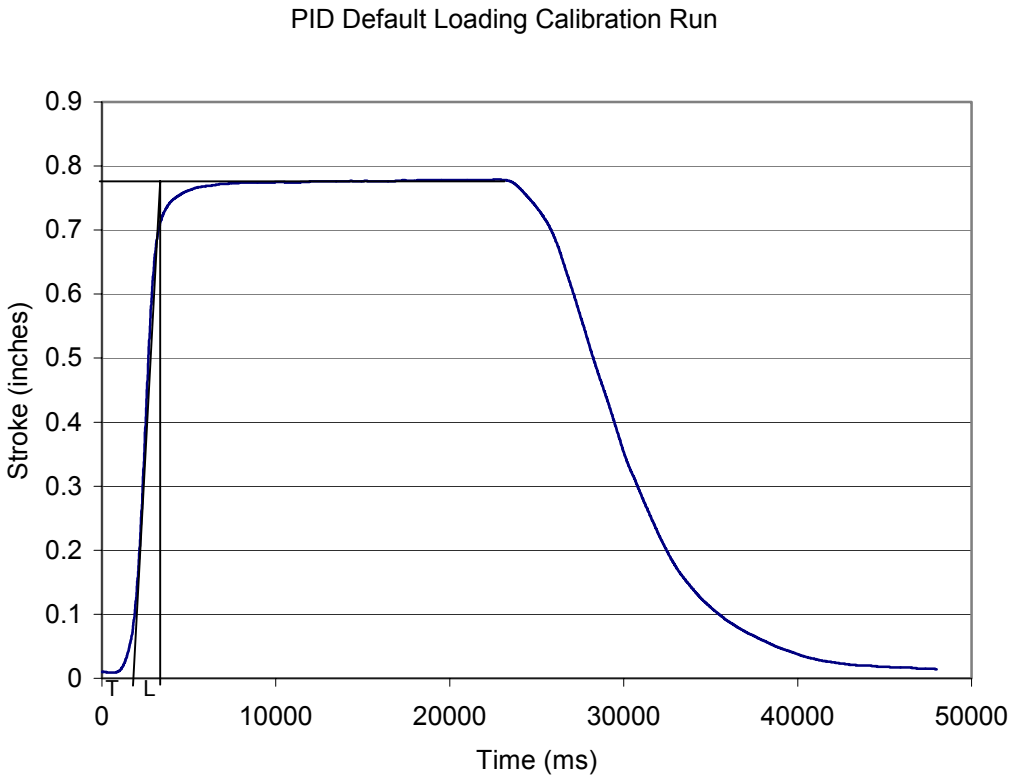

Figure 4.6 PID Default Loading Tuning Plot.

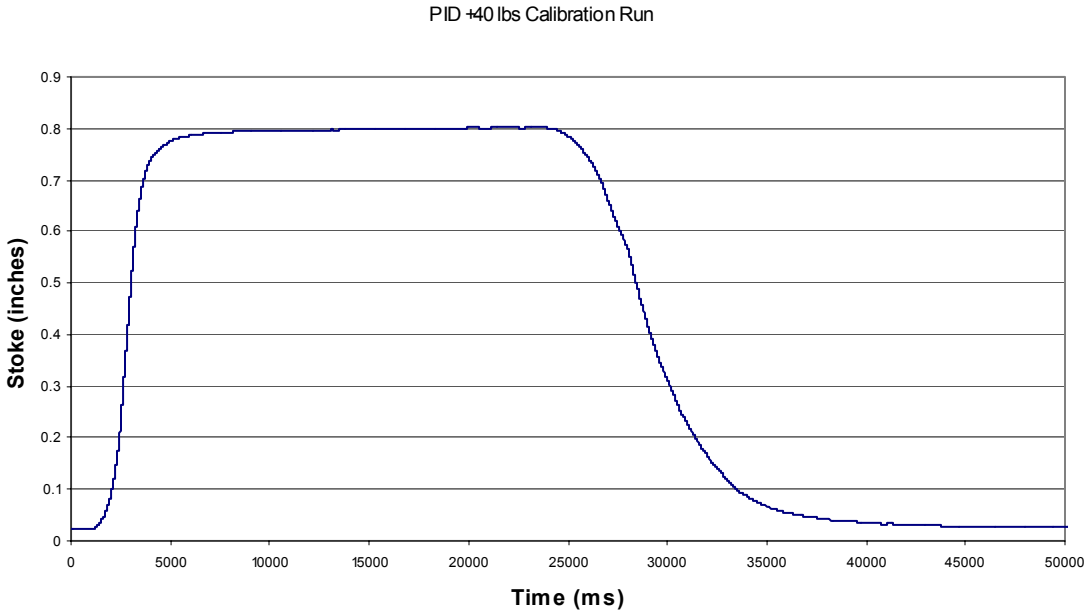

Figure 4.7 PID at +40 lbs Loading Tuning Plot.

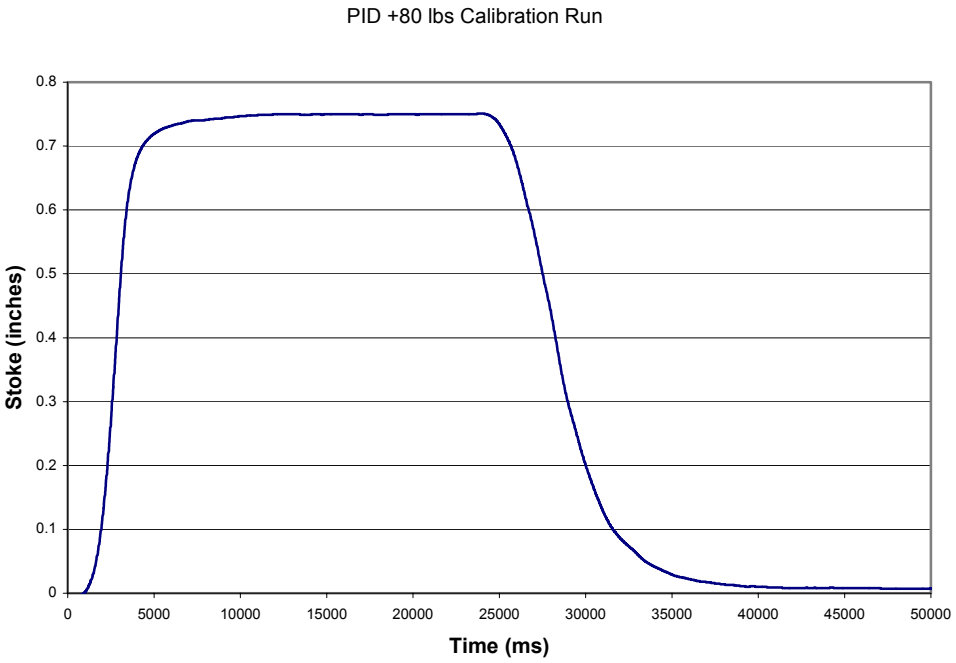

Figure 4.8 PID at +80 lbs Loading Tuning Plot

The T and L values were then obtained from the plot as seen in figure 4.6. Then the Kp, Ki and Kd constants were obtained as follows:

$$P: K_p = \frac{T}{L}$$

$$PI: K_p = 0.9\frac{T}{L} \qquad K_i = 0.27\frac{T}{L^2} \tag{4.1}$$

$$PI: K_p = 1.2\frac{T}{L} \qquad K_i = 0.6\frac{T}{L^2} \qquad K_d = 0.6T$$

These values were calculated for P, PI and PID controllers in the three different loading conditions. The obtained parameters are displayed in Table 4.1.

Table 4.1 PID, PI and P Constants for all Loading Cases.

		Default Loading	+40 lbs	+80 lbs
	L	1.1250	1.8200	1.5760
	T	2.9780	2.1320	2.1970
PID	Kp	3.1765	1.4057	1.6728
	Ki	1.4117	0.3861	0.5307
	Kd	1.7868	1.2792	1.3182
PI	Kp	2.3824	1.0543	1.2546
	Ki	0.6353	0.1738	0.2388
P	Kp	2.6471	1.1714	1.3940

Overall 27 runs were made. For each of the three loading conditions: default loading or 63 lbs as shown in the previous chapter, +40 and +80 a PID, PI and P controller was implemented. All these tests were also conducted for three different setpoints: 0.25, 0.50 and 0.75 inches. Results were compared in terms of loading conditions and setpoint.

Default loading

Responses for the default loading condition (63 lbs) are shown in Figure 4.9. The performance measurements are displayed in Table 4.2. Rise times for all the cases are relatively comparable. All the controllers overshot to the open loop step input response, between 0.75 and 0.80 inches, hence the scaleable percentage overshoot values for all the

setpoints. The proportional control failed at the 0.25” and 0.50” setpoints while the 0.75” case yielded an extremely high value of 67 sec for the settling time when compared to approximately 5 seconds for the PID and PI counterparts. At 0.25” and 0.50” setpoints there are mixed results between the PID and PI controllers. At 0.25” the PID controller bested the PI control by 3 seconds whereas at 0.50” the PI control performed 11 seconds better than the PID.

Table 4.2 Performance Measurements for Overall Response at Default Loading.

Default Loading					
	Controller	Rise Time (sec)	Peak Time (sec)	PO (%)	Settling Time (sec)
0.25"	PID	2.61	5.078	180.00%	36.014
	PI	3.191	6.071	196.40%	39.076
	P	3.328	6.995	168.80%	-
0.50"	PID	3.62	6.721	45.00%	44.267
	PI	3.704	8.587	47.20%	33.727
	P	3.644	6.59	45.20%	-
0.75"	PID	4.728	10.632	1.47%	4.728
	PI	4.946	39.193	1.20%	4.946
	P	4.98	6.885	-3.47%	66.83

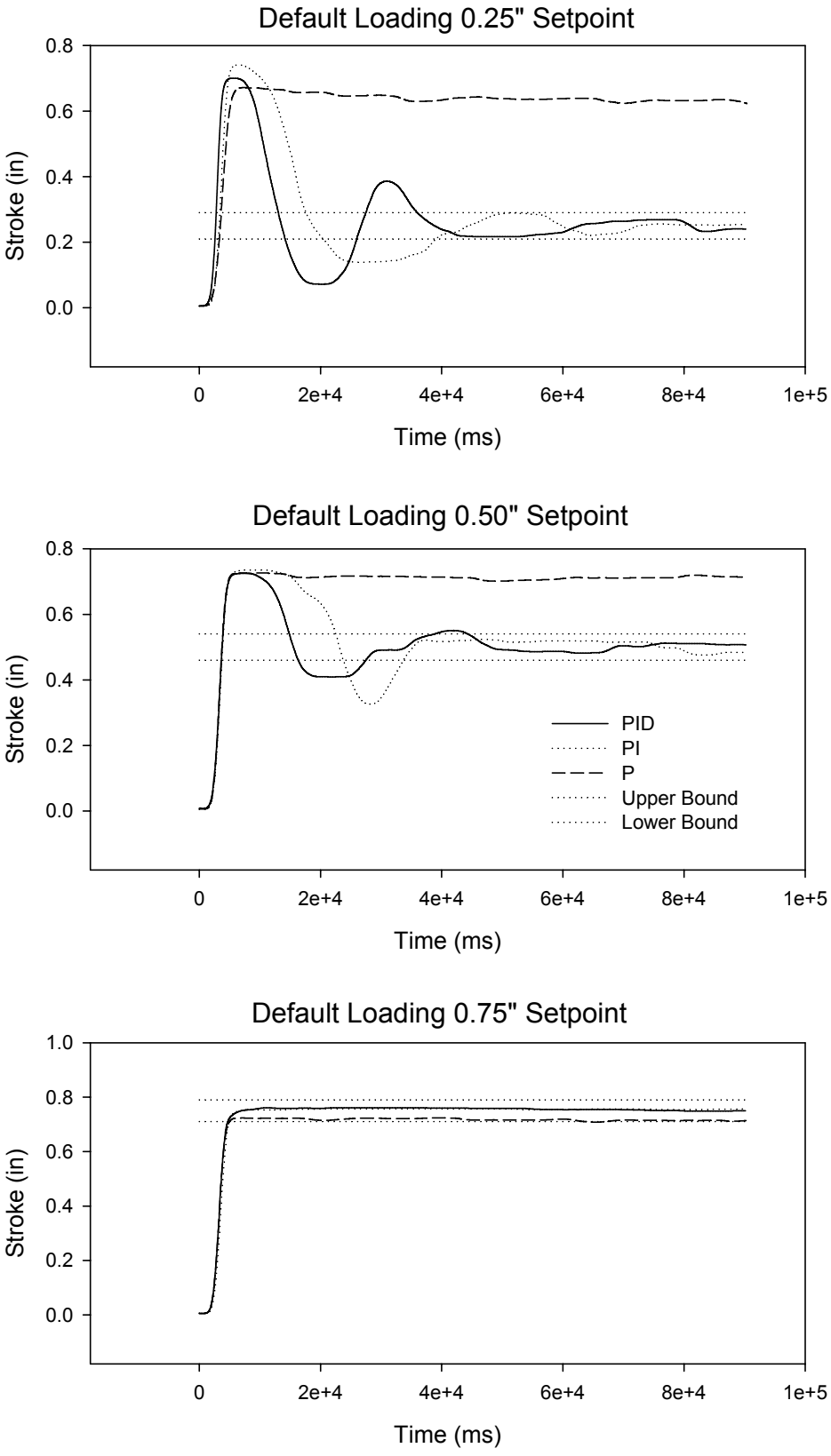

Figure 4.9 Overall Close Loop Response at Default Loading.

+40 lbs Loading

Figure 4.10 displays the response for all the setpoints and controllers at the +40 lbs loading condition, while Table 4.3 summarizes its performance measurements. The effect of the added mass results in a degradation of the response of the system. This can be seen clearly in the rise times, which are approximately one second higher than their counterparts in the default loading case. The percentage overshoot values remained relatively unchanged from those for the default loading case. Settling times however increased significantly from the previous case. The PID and PI controllers provided mixed results like before at the 0.25" and 0.50" setpoints, while the P controller failed to stay within the control boundary. All the controllers provided similar results at the 0.75" setpoint, something that is expected since is close to the maximum possible response for this setup.

Table 4.3 Performance Measurements for Overall Response at +40 Loading.

+40 lbs Loading					
	Controller	Rise Time (sec)	Peak Time (sec)	PO (%)	Settling Time (sec)
0.25"	PID	3.16	8.02	194.80%	136.544
	PI	3.094	7.892	200.00%	107.76
	P	3.61	89.128	195.20%	-
0.50"	PID	4.302	11.976	47.80%	51.36
	PI	4.256	13.916	47.60%	97.548
	P	4.332	33.24	49.80%	-
0.75"	PID	5.878	24.904	2.13%	5.878
	PI	5.274	100.024	1.60%	5.274
	P	5.97	180.846	0.67%	5.97

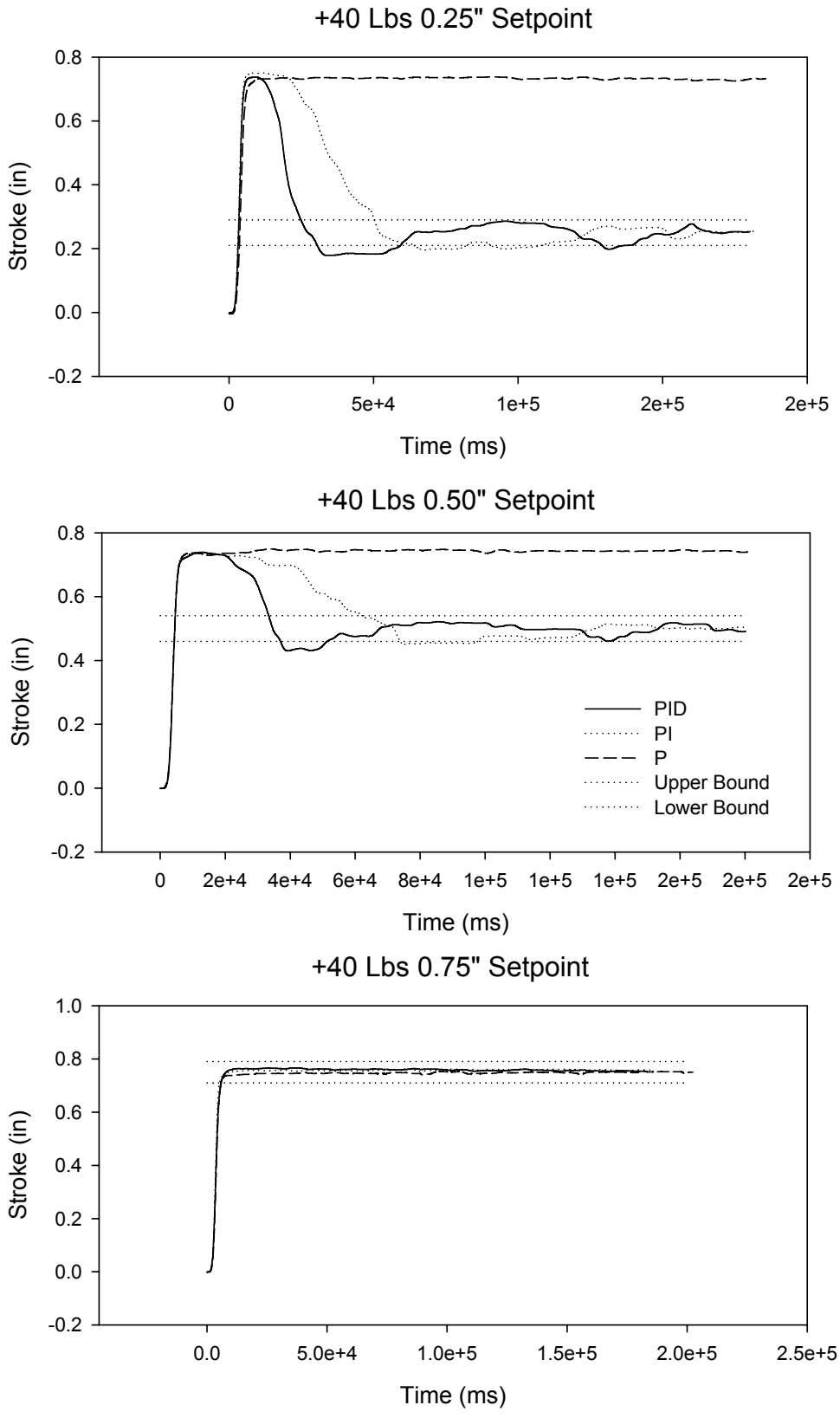

Figure 4.10 Overall Close Loop Response at +40 lbs Loading.

+80 lbs Loading

For this case additional response degradation can be observed from the rise, peak and settling times, which are shown in Table 4.4. Overall behavior remained relatively unchanged from previous loading cases with the exception being the response for the PID and PI controllers at the 0.50" case. As shown in Figure 4.11, at 0.50" setpoint appreciable oscillations can be noted for the PID and PI controllers. This can be due in part to the nature of the additional loading in the form of the constant force springs.

Table 4.4 Performance Measurements for Overall Response at +80 Loading.

+80 lbs Loading					
	Controller	Rise Time (sec)	Peak Time (sec)	PO (%)	Settling Time (sec)
0.25"	PID	3.204	6.9	173.60%	72.636
	PI	3.116	7.232	186.00%	39.404
	P	3.344	29.848	191.60%	-
0.50"	PID	4.056	10.328	43.00%	55.098
	PI	3.912	10.398	44.40%	153.82
	P	4.022	58.652	46.40%	-
0.75"	PID	6.492	120.774	0.13%	6.492
	PI	6.07	79.112	-0.67%	6.07
	P	6.088	69.84	-3.20%	6.088

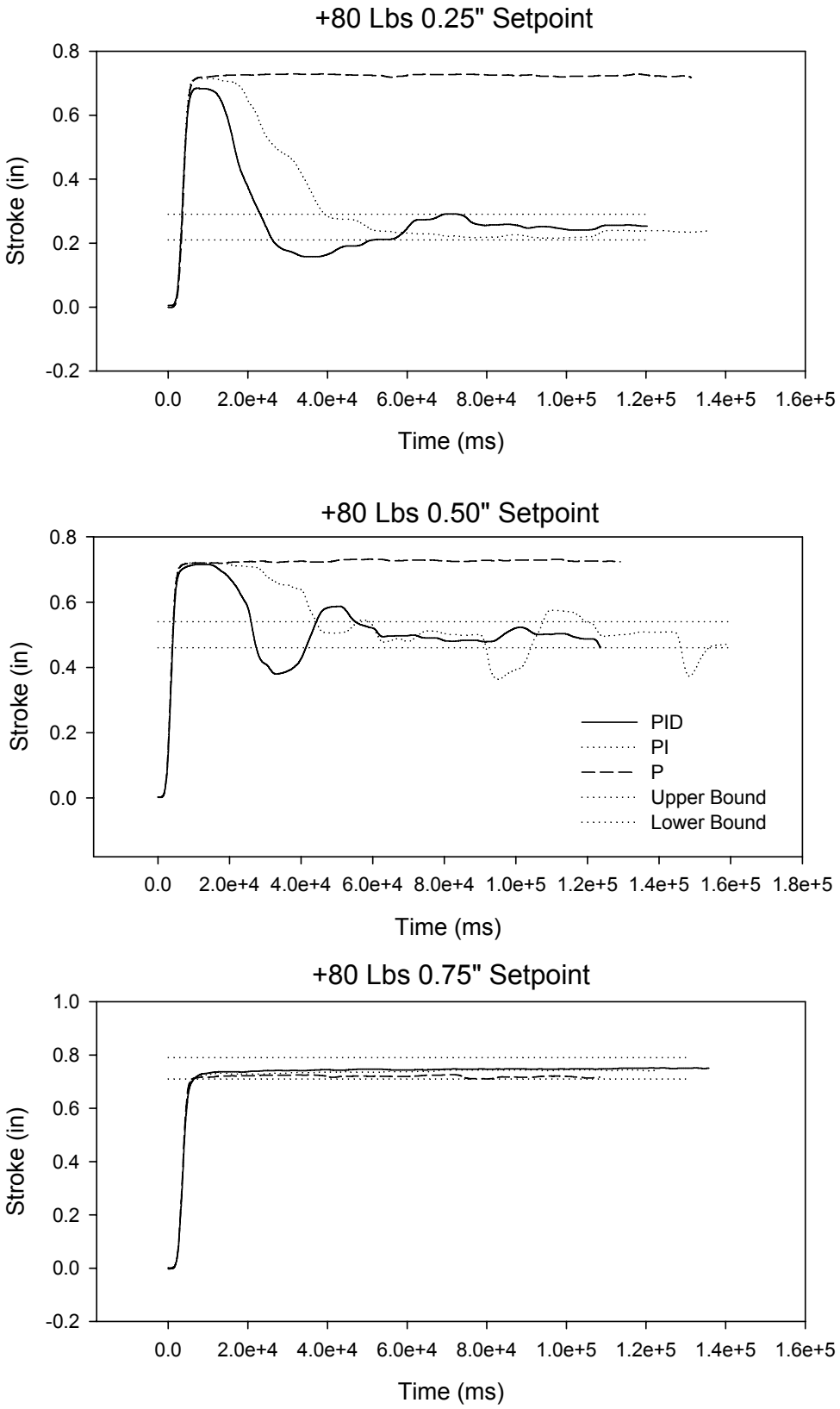

Figure 4.11 Overall Close Loop Response at +80 Loading.

Optimized case

The results shown in Figures 4.9 thru 4.11 illustrate the response of the actuator for PID constants tuned using the Nichols method. For these previous cases the parameters were different for each of the loading conditions. For this case, however the actuator was tested with a unified Nichols tuned PID and these values were compared to an optimized PID controller. The tuned parameters were obtained from the middle case that is, +40 lbs and 0.50" setpoint. The Nichols parameters were recalculated for this test and are as follows: Kp = 1.68, Ki = 0.672, and Kd = 1.05. The Optimized constants are as follows: Kp = 11.7, Ki = 0.57, and Kd = 11. The actuator was then tested at all the loading conditions and setpoints for the two PID constants sets. The results are divided by setpoint condition.

At 0.25" setpoint

The results for this case are displayed in Figure 4.12 and the performance measurements are tabulated below. Percentage overshoot was reduced for all the loading conditions by an average of 100% less for the optimized case. These reductions in the PO lead to lower settling times for all the cases as well. The highest improvement was made at 40 lbs with a reduction in the settling time of approximately 62 seconds. At 80 lbs the optimized case gained 38 seconds and in the default loading case a gain of 40 seconds was observed.

Table 4.5 Nichols - Optimized Performance Measurements at 0.25” Setpoint.

0.25" Setpoint					
	Controller	Rise Time (sec)	Peak Time (sec)	PO (%)	Settling Time (sec)
Def.	Nichols	2.806	6.728	200.00%	58.402
	Optimized	2.868	4.624	114.40%	18.012
+40	Nichols	4.379	8.801	192.80%	72.206
	Optimized	3.324	4.906	86.40%	10.295
+80	Nichols	3.257	7.427	181.20%	48.629
	Optimized	3.276	4.7	86.40%	10.292

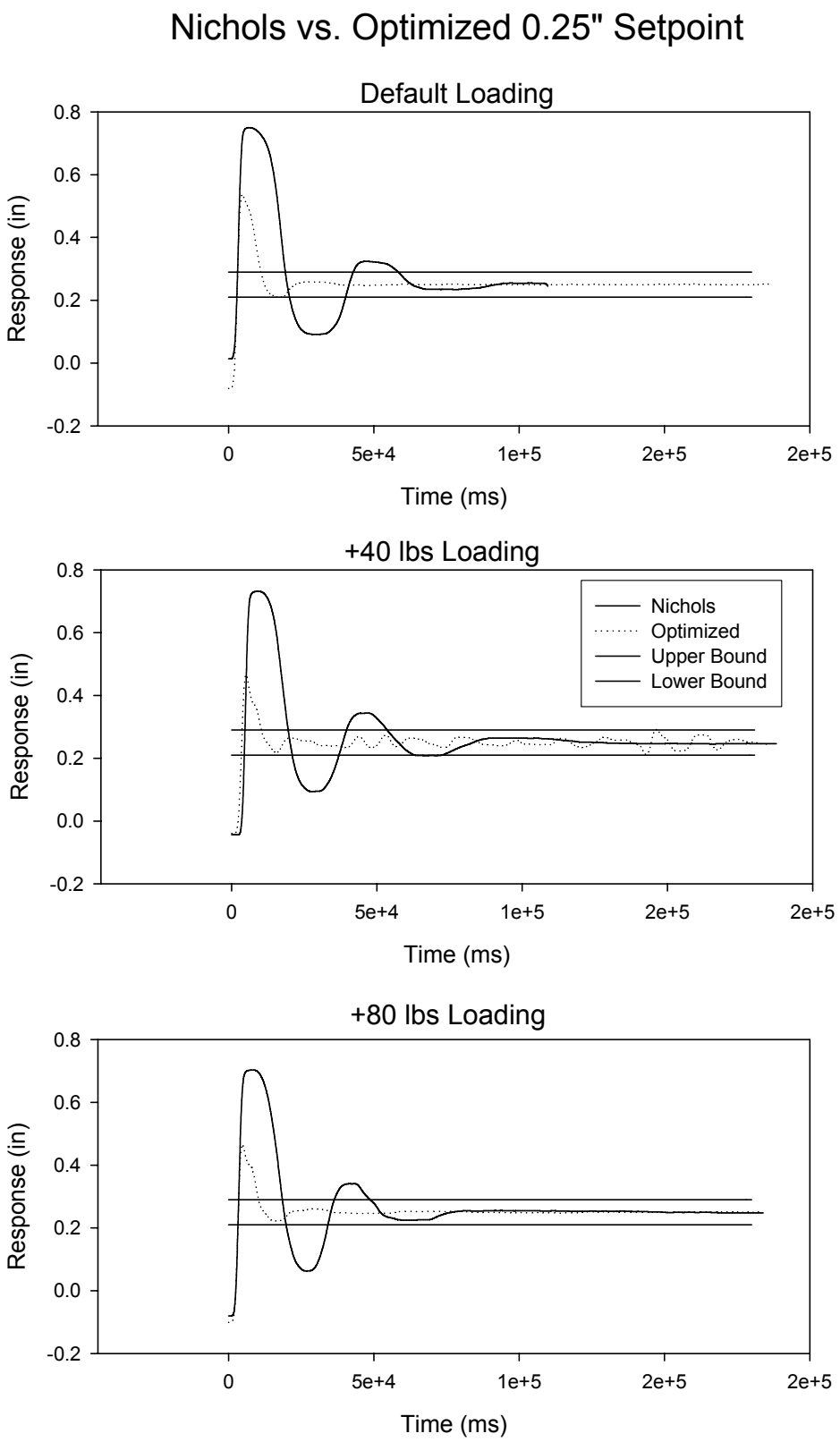

Figure 4.12 Nichols vs. Optimized at 0.25" Setpoint.

At 0.50” setpoint

The response at this setpoint is displayed in Figure 4.13. The +40 lbs optimized yielded the best response at this setpoint. This is expected since the optimization was made at 40 lbs for a setpoint of 0.50”. Any increase or reduction from the +40 lbs results in a slower response. The difference from the +40 case to the other two cases in the settling time is about 8 seconds. The average increase in percentage overshoot from the +40 case is about 19%.

Table 4.6 Nichols - Optimized Performance Measurements at 0.50” Setpoint.

0.50" Setpoint					
	Controller	Rise Time (sec)	Peak Time (sec)	PO (%)	Settling Time (sec)
Def.	Nichols	3.732	7.576	53.40%	46.768
	Optimized	3.774	4.984	20.80%	12.36
+40	Nichols	4.412	8.841	50.60%	52.668
	Optimized	4.268	9.042	7.00%	4.268
+80	Nichols	3.866	8.13	42.80%	39.629
	Optimized	4.132	9.364	13.00%	11.934

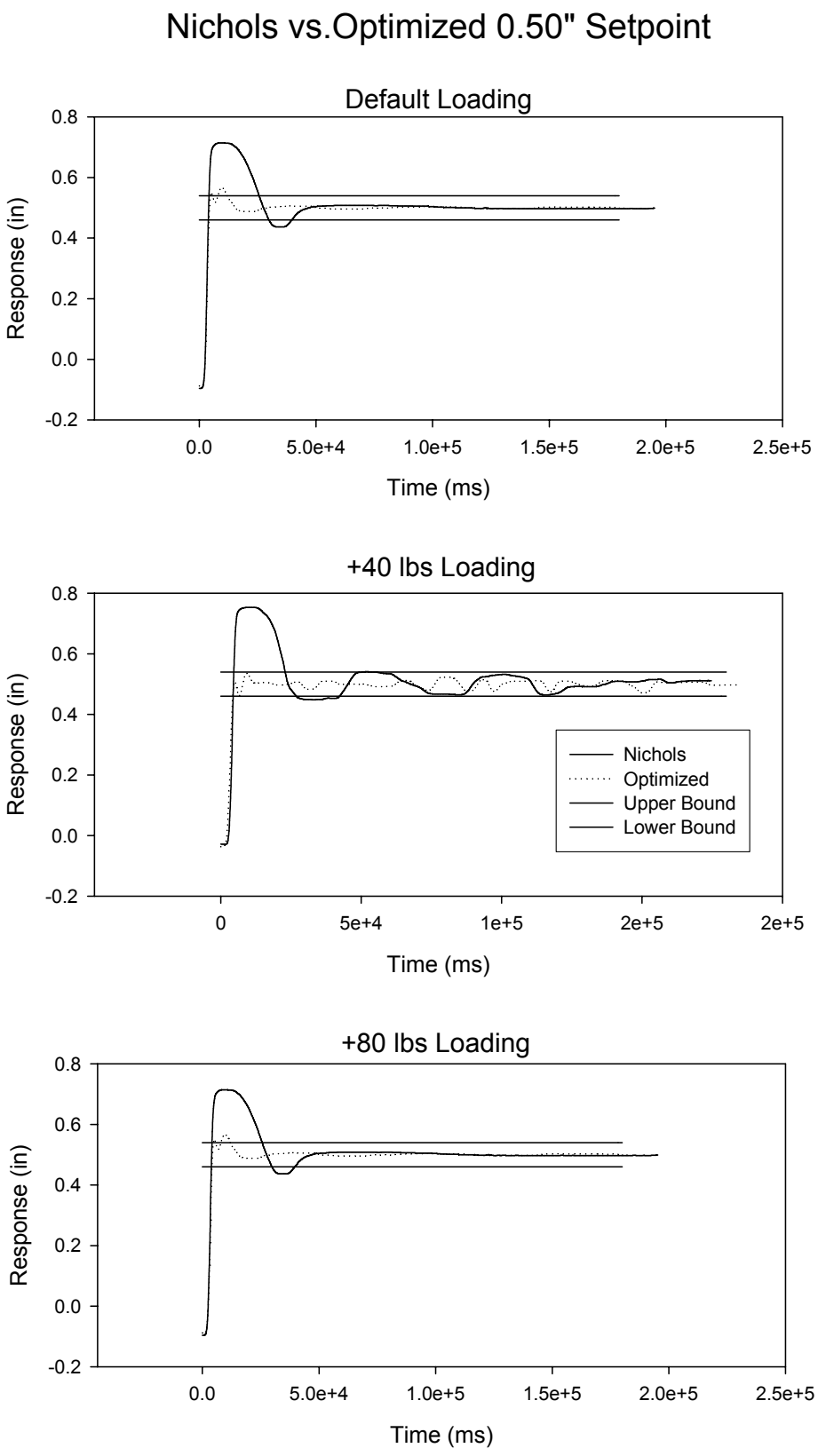

Figure 4.13 Nichols vs. Optimized at 0.50" Setpoint.

At 0.75" setpoint

The 0.75" setpoint is the only case where the Nichols PID bested the optimized one. To reduce the percentage overshoot the optimized PID was overdamped. This does translate into a faster settling time when any overshoot is possible. However, for this case since the setpoint is close to the maximum stroke possible for this setup little or no overshoot will be observed. The Nichols PID achieved control faster simply because an overdamped system will take more time to rise. This does not signify that the Nichols PID is recommended for a case where the setpoint is close to the maximum since if this is the type of actuation desired then a simple open loop response will suffice.

Table 4.7 Nichols – Optimized Performance Measurements at 0.75" Setpoint.

0.75" Setpoint					
	Controller	Rise Time (sec)	Peak Time (sec)	PO (%)	Settling Time (sec)
Def.	Optimized	4.316	28.2	3.47%	4.316
	Nichols	9.656	50.92	0.67%	9.656
+40	Optimized	4.926	32.99	1.60%	4.926
	Nichols	11.465	38.816	0.80%	11.465
+80	Optimized	6.083	125.258	0.80%	6.083
	Nichols	11.428	108.532	0.53%	11.428

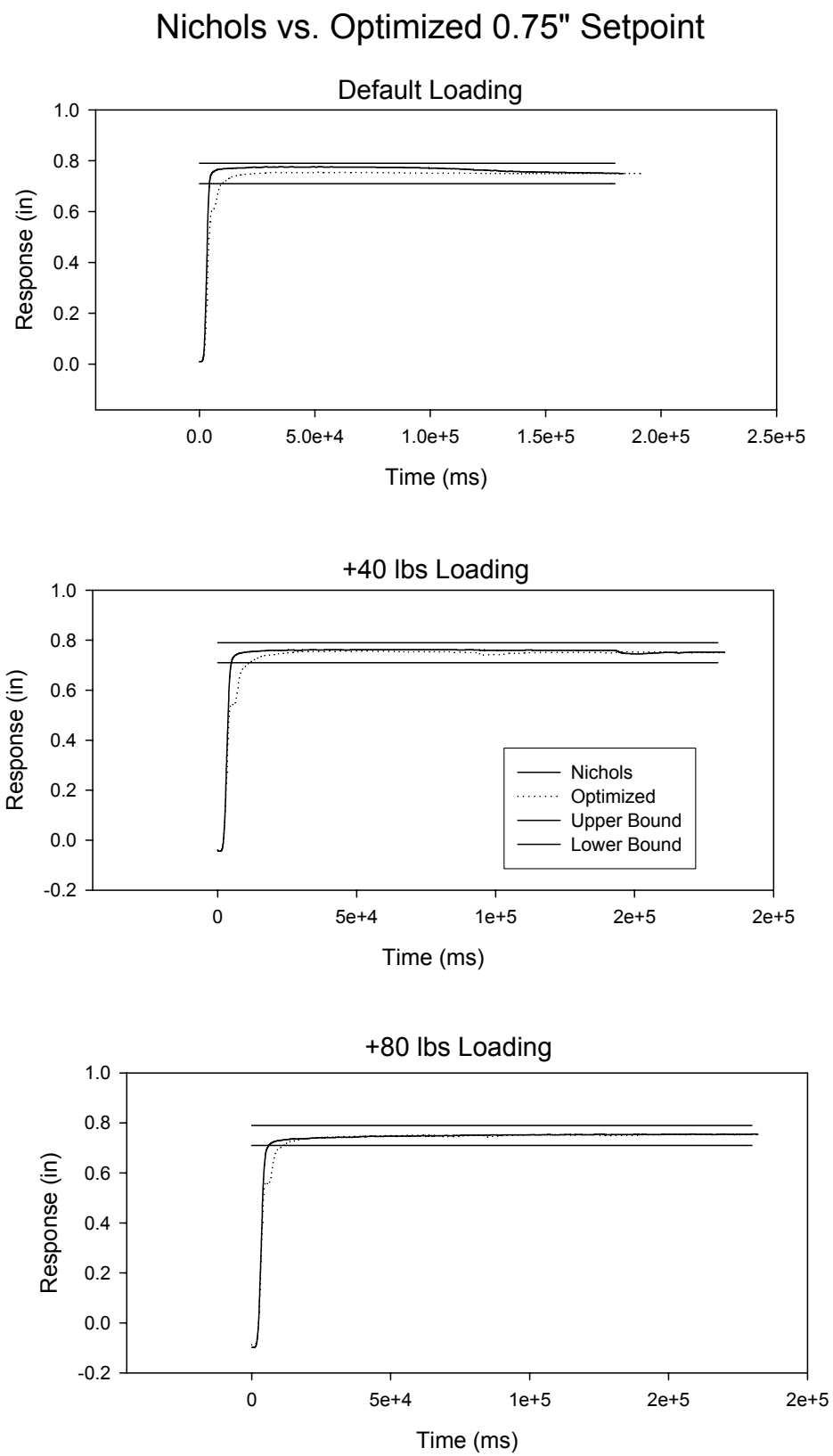

Figure 4.14 Nichols vs. Optimized at 0.75" Setpoint.

CHAPTER 5
CONCLUSIONS

SMA Correlations

Suffice to say that SMA related design is not an easy endeavor. Several aspects must be considered before the final prototype takes place. One of the major obstacles to overcome are the intertwined properties of shape memory alloys. Most of the physical, electrical and mechanical aspects of shape memory depend on each other and at some point design decisions must be make to reduce the number of variables. In reality a trade back is always made. Some of these correlations are discussed next.

Force vs. Cycle Times vs. Power:

As discussed in chapter three of this work the actuation force that a shape memory element is capable of is a function of its cross-sectional area. For a straight wire this means a circular cross sectional area. The actuation cycle of a shape memory element is a function of the heating and cooling times, which is a function of the heat transfer phenomena inside the SMA which in turn has one of its parameters the cross sectional area of the element. Without getting into specifics we know that the higher the cross sectional area of an element the longer it will take to cool down and this will lead to a higher actuation cycle. Based on this we know that the force of the element is directly proportional to the time it takes the actuator to complete one full cycle. If the force required by the SMA element is large then expect to see a slower actuator.

This drawback can be addressed by the implementation of a parallel configuration of shape memory elements, such as the one implemented in this work. The parallel array

of wires can provide a higher force while maintaining a fast enough response. This however, posses another factor to consider: power. Large cross sectional area shape memory alloy elements are typically more efficient than lower ones, thus a trade back is presented to the designer: which design factor is more important? If the designer is more interested solely in force and a simplified design then a large element or a small bundle of large elements can be considered at the expense of a slower response but with more efficient wires. However if the most important factor to consider is the response time of the actuator then a bundle of wires in parallel configuration to provide for the force at the expense of more power needed to drive the device. Since shape memory alloys are inherently inefficient it is recommended that the designer explore how much can be gained by sacrificing the actuation times.

Stroke vs. Durability vs. Envelope Volume

As previously stated in Chapter 3 the stroke of a shape memory element is a function of the strain the actuator is subject to. The most typical maximum strain that a SMA can exert is in the vicinity of 8%. However, this value if implemented will lead to less than 100 cycles after which the performance of the element will start to degrade. The lifetime cycles can be greatly improved if the working strain is to be reduced. Previous work has concluded that for Nitinol a strain of 5% will yield hundreds of thousands of cycles, and the cost of a higher lifetime is a reduced actuation stroke. Another factor that ties into this equation is the overall length of the shape memory element, which is also a function of the stroke. The length is a factor of the envelope volume where the actuator resides. The designer must then consider which one of these parameters is more important in its design and a trade back will be made.

Advantages and Drawbacks

As of today there are few advantages for implementing a shape memory driven actuator, especially for large-scale applications. The most attractive features reside in a compact design, low weight and minimal sound levels. Design wise their implementation at large scale is a difficult process to say the least. Power consumption is extremely high when compared to technologies that can provide the same level of functionality. However, they do offer a viable alternative to hydraulics, which is the method of choice when handling large loads. Their inherent low weight makes them ideal for portable designs and space exploration.

Control Aspects

This work showed that a large-scale SMA actuator is possible and although far from perfect the actuator can be controlled within reason. The following discusses the conclusions that were derived from testing.

1. Open loop response was repeatable and precise.
2. The output from the open loop produced a response from which Nichols tuning method can be implemented for latter use in the closed loop.
3. The steady state open loop response produced the same trend as a SMA stress strain chart.
4. Open loop case serves as an ideal implementation when only one setpoint is desired or an on/off application.
5. Time response for the open loop was around 4-5 seconds for all loading conditions.
6. A proportional controller alone cannot be used to control a shape memory based actuator. Proportional control only achieves acceptable response under the 0.75” setpoint, slightly less than the maximum stroke defined for the setup.
7. PI and PID control schemes yielded similar responses, with the PID solution having better overall responses. This indicates that the system does in fact benefit from the damping effect of the derivative controller.

8. Optimization for a PID controller is achievable and in the implemented optimized case the maximum performance obtained varied from a Nichols tuned PID by as much as 1300%.

Viability

A large-scale implementation of shape memory alloys although possible can become an expensive endeavor. The cost alone of the shape memory elements indicates that the system will be expensive but it also depends on the number of elements being used. Custom design of shape memory elements is far more expensive than pre made commercial ones. Case in point a single strip of Ni-Ti custom made would cost around 2000 dollars. If cost is an important factor then the commercial available forms and sizes should be implemented and the design adjusted to accommodate to this element.

CHAPTER 6
FUTURE WORK

Although some headway was made for future work in this area the implementation of SMA for large-scale control is still far from reality. The major benefit a future researcher in this area can expect from this work comes in the form of its extensive but practical literature review as well as pointing out possible design strategies while avoiding some of the most time consuming pitfalls.

In terms of a practical and easy to implement actuator the design of a small stroke actuator with a large actuation force would be a possibility while reciprocating some of the force to an increased motion. Work has been done on this area by Gorbet [14] but the force of his actuator has been limited.

Another possible and practical design to achieve high force and stroke can be obtained by implementing a rotational shape memory alloy driven rotational actuator coupled with a linear bearing spline to achieve the desired stroke. These design strategies call for the SMA units to be actuated as an on/off device thus avoiding the complex control at the material level.

Then there is always the most common implementation of shape memory devices in the form of micro actuators, an area where these materials have already proven their worth.

LIST OF REFERENCES

1. J. Van Humbeeck, and Jan Cederstrom, "The Present State of Shape Memory Materials and Barriers Still to be Overcome," *Proceedings of the 1st International Conference on Shape Memory and Superelastic Technologies (SMST-94)*, 7-10 March 1994, Asilomar Conference Center, Pacific Grove, California, USA, SMST, Santa Clara, CA, 1994, pp. 1-6.

2. H. Funakabo, ed. translated from Japanese by J.B. Kennedy, S*hape Memory Alloys*, Gordon and Breach Science Publishers, Amsterdam, Holland, 1987.

3. T.W. Duerig, C. M. Wayman, "An Introduction to Martensite and Shape Memory," *Engineering Aspects of Shape Memory Alloys*, Butterworth-Heinemann Publishers, London, 1990, pp. 3-20.

4. J. Perkins, and D. Hodgson, "The Two Way Shape Memory Effect," *Engineering Aspects of Shape Memory Alloys*, Butterworth-Heinemann Publishers, London, 1990, pp. 195-206.

5. Jorma Ryhanen Ph.D. "Biocompatibility Evaluation of Nickel-Titanium Shape Memory Metal Alloy", Thesis, Oulu University, Finland, (1999), Available in PDF format online at: http://herkules.oulu.fi/isbn 9514252217/ , accessed 5/22/2001.

6. K. Otsuka, "Introduction to the R-Phase Transition," *Engineering Aspects of Shape Memory Alloys*, Butterworth-Heinemann Publishers, London, 1990, pp. 36-45.

7. Y. Suzuki, and H. Tamura, "Fatigue Properties of Ni-Ti Shape Memory Alloys," *Engineering Aspects of Shape Memory Alloys*, Butterworth-Heinemann Publishers, London, 1990, pp. 256-266.

8. T.W. Duerig, and G.R. Zadno, "An Engineer's Perspective of Pseudoelasticity," *Engineering Aspects of Shape Memory Alloys*, Butterworth-Heinemann Publishers, London, 1990, pp. 369-393.

9. T. C. Waram, 2nd Edition, *Actuator Design Using Shape Memory Alloys*, T.C.Waram, Hamilton, Ontario, 1993.

10. R.G. Gilbertson, 3rd Edition, *Muscle Wires Project Book*, Mondo-tronics, Inc., San Anselmo, CA., 1994.

11. T. Waram, "Design Principles for Ni-Ti Actuators," *Engineering Aspects of Shape Memory Alloys*, Butterworth-Heinemann Publishers, London, 1990, pp. 234-244.

12. R.C. Juvinall, and K.M. Marshek, 2nd Edition, *Fundamentals of Machine Component Design*, John Wiley and Sons, Inc., NY, 1991, p.427-452.

13. Y. Nakano, M. Fujie, and Y. Hosada, "Hitachi's Robot Hand," *Robotics Age*, vol. 6, no. 7, July 1984, pp. 18-20.

14. R.B. Gorbet, and R.A. Russell, "A Novel Differential Shape Memory Alloy Actuator for Position Control," *Robotica*, vol. 13, Cambridge University Press, Cambridge, UK, 1995, pp. 423-430.

15. D Grant, V. Hayward, "Design of Shape Memory Alloy Actuator with High Strain and Variable Structure Control," *Proceedings of 1995 IEEE International Conference on Robotics and Automation, Nagoya, Japan*, vol. 3, 1995, pp. 2305-2310.

16. A.B. Soares, H.M. Brash, and D. Gow, "The Application of SMA in the Design of Prosthetic Devices," *Proceedings of the 2nd International Conference on Shape Memory and Superelastic Technologies (SMST-97)*, 2-6 March 1997, Asilomar Conference Center, Pacific Grove, California, USA, SMST, Santa Clara, CA, 1997, p. 257-262.

17. M. Mosley, and C. Mavroidis, "Design and Dynamics of A Shape Memory Alloy Wire Bundle Actuator," *Proceedings of the 2000 ASME Mechanisms and Robotics Conference*, Baltimore MD, September 10-13, 2000.

18. John Van de Vegte, 3rd Edition, *Feedback Control Systems*, Prentice Hall, NJ, 1994, pp. 146-147

BIOGRAPHICAL SKETCH

José R. Santiago was born on December 16, 1973, in the town of Ponce, Puerto Rico. After graduating from high school he attended the University of Puerto Rico Mayagüez Campus, where he obtained a Bachelor of Science in mechanical engineering on 1997. In 1998 he enrolled in the graduate program of the University of Florida to pursue a master's degree in mechanical engineering. His focus while in this program has been towards shape memory alloys, machine design, rapid prototyping, computer aided design and application programming. During this period he has been a Teaching Assistant for EML 3023 Computer Aided Design and EML 3005 Introduction to Machine Design Currently he holds a research assistantship at the Center for Intelligent Machines and Robotics (CIMAR) and is working on barrel packing algorithms.